Journal of Hazardous Materials Advances 18 (2025) 100742

Contents lists available at ScienceDirect

Journal of Hazardous Materials Advances

journal homepage: www.elsevier.com/locate/hazadv

Removal of refractory organic compounds from water by adsorption using carbon xerogel cylinders coupled with *in situ* regeneration using H_2O_2 electro-generation and UV radiation

Julien G. Mahy [a,b,*], Hamed Arab [b], Marthe Kiendrebeogo [b], Antoine Farcy [a], Tom Servais [a], Alexandre Léonard [a], Patrick Drogui [b]

[a] Department of Chemical Engineering, Nanomaterials, Catalysis & Electrochemistry, University of Liège, Allée du Six Août 11, 4000 Liège, Belgium
[b] Centre INRS – Eau, Terre, Environnement (INRS-ETE), Québec, Canada

ARTICLE INFO

Keywords:
Quaternary water treatment
3D porous carbon
Electro-photocatalysis
Adsorption, sol-gel process
Micropollutant degradation
Electrochemical regeneration

ABSTRACT

The process developed in this study is based on the adsorption of refractory organic compounds (ROCs) onto carbon xerogels, coupled with *in situ* regeneration of the adsorbent by H_2O_2 electro-generation and enhanced ROC decomposition via OH radicals due to UV illumination. The *in situ* regeneration of the carbon materials aims to replace the usual thermal regeneration, which is costly and gradually degrades the adsorption properties. In this work, carbon xerogels are synthesized via a sol-gel process and molded as cylinders that are used as adsorbents for ROCs. The specific surface area of these cylinders varies between 30 and 680 m^2/g when the resorcinol/sodium carbonate (*R/C*) ratio is modified between 100 and 1500 during the synthesis. Their excellent adsorption properties are highlighted for three model pollutants (*i.e.*, p-nitrophenol, methylene blue, and ibuprofen), and it is determined that the optimal cylinders have an *R/C* ratio of 750. In parallel, the electro-generation of H_2O_2 within these cylinders is demonstrated, reaching an H_2O_2 concentration of 5 mg/L when using the most porous carbon cylinder (*i.e.*, the optimal one). The use of UV light combined with the electro-generation of H_2O_2 enables the efficient production of hydroxyl radicals. Finally, *in situ* regeneration of the optimal saturated carbon cylinders for the model pollutants is successfully performed. Indeed, the results of carbon cylinder regeneration for the three pollutants show that the H_2O_2 electro-generation combined with the UV illumination completely mineralized the three pollutants previously absorbed on the carbon cylinders. These promising results open the way for a new method that regenerates adsorbent materials *in situ* without the use of thermal treatments.

1. Introduction

Freshwater resources barely represent 1 % of all water on the planet (Corson-Dosch et al., 2023). However, the scarcity of this irreplaceable resource, although largely renewable, is raising growing concerns, exacerbated by the major challenges of our time, such as growing demographic pressures, changes in lifestyles, and extensive consumption. Furthermore, climate change amplifies the severity of these interconnected challenges (United Nations Educational 2021; UNESCO 2022). Currently, more than two billion people are deprived of direct access to water or face shortage or quality problems, highlighting the insufficiency and need for improvement of sanitation systems (Ammar 2023). As water management is a matter of ethics and international law, it is imperative to find approaches that increase the quantity and quality of water resources via the decontamination of wastewater and its reuse. Due to recent advances in analytical techniques for detecting minimal quantities of substances (Adeleye et al. 2022), micropollutants present at the exit of wastewater treatment plants (WWTPs) are now attracting increasing attention. These substances, present for years in wastewater, surface water, groundwater, soil, and aquatic organisms, exhibit highly diverse forms such as dyes, aromatics, pesticides, solvents, EDCs (endocrine disrupting chemicals), PFAs (as perfluorooctanesulfonic acid (PFOS)), and PPCPs (pharmaceuticals and personal care products) causing disturbances to aquatic life and create risks to human health (Turolla et al. 2012; Scholz 2016; Adeleye et al. 2022). These pollutants mostly escape conventional WWTPs and can be found at their exit in

* Corresponding author.
E-mail address: julien.mahy@uliege.be (J.G. Mahy).

https://doi.org/10.1016/j.hazadv.2025.100742
Received 22 January 2025; Received in revised form 27 April 2025; Accepted 7 May 2025
Available online 8 May 2025

very low concentrations (µg/L), which explains the name of micropollutants or refractory organic compounds (ROCs). Even if these ROCs represent very low quantities, several studies show that these compounds can pose a threat to water sources and present health risks (Gutkoski et al. 2024). The diverse variety of these molecules (Undeman et al. 2022) makes their elimination more challenging and, thus, requires a process combining different degradation techniques that mostly ensures complete destruction of these ROCs (Mahy et al. 2019b).

Chemical treatments can be used to decontaminate wastewater with reagents such as chlorine, H_2O_2, or O_3 (Trevelin et al. 2023; Trench et al. 2023; Sanavi Fard et al. 2023a). This process is efficient for degrading some pollutants but it is costly, may generate hazardous compounds, and needs a constant supply of chemicals (Trevelin et al. 2023; Trench et al. 2023; Sanavi Fard et al. 2023a). An alternative to these chemical treatment processes, which is currently under study, is the direct production of H_2O_2 via water electrolysis with a two-electrode cell (Guitaya et al. 2015; Kiendrebeogo et al. 2022; Trevelin et al. 2023; Trench et al. 2023). H_2O_2, which can be electrochemically generated at the cathode (made of carbon, usually a graphite cell) (Guitaya et al. 2015; Kiendrebeogo et al. 2022; Trevelin et al. 2023; Trench et al. 2023), is an environmentally metastable molecule. Indeed, H_2O_2 provides strong disinfecting and oxidizing properties and is able to convert toxic organics into less harmful molecules (Guitaya et al. 2015; Kiendrebeogo et al. 2022; Trevelin et al. 2023; Trench et al. 2023). However, H_2O_2 can be ineffective when attempting to degrade some organic molecules (Mahy et al. 2023) but, in the present case, its conversion into hydroxyl radicals (•OH) greatly assists the degradation of these pollutants. Several techniques are possible for converting H_2O_2 into •OH, such as the use of a metal catalyst (mainly composed of iron (Zhang et al. 2023a)) or exposure to UV radiation (Mahy et al. 2023). The combination of H_2O_2 and O_3, known as the peroxone process, is a powerful process that degrades ROCs due to the presence of both of these oxidizing molecules and, in addition, OH radicals are formed via the reaction between them (Sanavi Fard et al. 2023a). This process needs a constant supply of both chemicals.

Over the past few decades, advanced oxidation processes (AOPs) have shown potential for use in wastewater decontamination (Oturan and Aaron 2014; Bashir et al. 2024; Din and Khalid 2025). These treatments are based on the *in situ* generation of a powerful oxidizing agent, such as •OH, at a sufficient concentration to efficiently decontaminate water (Kiendrebeogo et al. 2022; Mahy et al. 2023; Bashir et al. 2024). In AOPs, various methods have been established for the sustainable removal of a large range of organic pollutants, such as via H_2O_2/Fe^{2+} (Zhang et al. 2023b), O_3/OH^- (ozonation) (Issaka et al. 2022), UV only, H_2O_2/UV (Sanavi Fard et al. 2023b), O_3/H_2O_2 (Sanavi Fard et al. 2023a), H_2O_2/Fe^{3+}/UV (Brovini et al. 2023), electrochemical processes (Hu et al. 2021; Kiendrebeogo et al. 2022; Trench et al. 2023) (anodic oxidation, electro-Fenton), etc. Among AOPs, photocatalysis is highlighted as an efficient and promising process for the degradation of various organic compounds (Bashir et al. 2024). Nevertheless, this process requires the continuous illumination of the catalyst to generate the active species (Mahy et al. 2016).

Among the quaternary decontamination processes, the adsorption onto porous carbon materials seems to be the most efficient technique for ROCs removal (Karaca et al. 2008; Páez et al. 2012; Ferrández-Gómez et al. 2023), *i.e.*, via adsorption column filled with carbon pellets with very simple geometries. This process presents many advantages compared with other technologies, such as lower initial costs, simplicity of design and operation, and insensitivity to toxic substrates (Karaca et al. 2008; Páez et al. 2012; Wolfs et al. 2022; Ferrández-Gómez et al. 2023). Among carbon materials, activated carbons have the highest adsorption capacity for various ROCs (Yu et al. 2009; Ip et al. 2010; Páez et al. 2012; Wolfs et al. 2022) and, thus, are most commonly used. Among activated carbon, carbon xerogels are porous carbons obtained by sol-gel synthesis resulting from polycondensation of resorcinol and formaldehyde in water (Karaman et al. 2024), followed by drying and pyrolysis. This carbon material synthesis is an efficient method to produce carbon materials with a high specific surface area and a controlled *meso*/macro/micropore texture just by adapting the synthesis parameters and by activation (Job et al. 2004; Páez et al. 2012; Karaman et al. 2024) to reach high specific surface areas (up to 2000 m^2/g). Moreover, their shaping to specific geometries is easily achieved via 3D printing (Wolfs et al. 2022). Thus, carbon xerogels are interesting model materials for studying adsorption, especially since they can be shaped for electrochemical applications.

One of the main drawbacks of current adsorption processes with carbon materials is the need for thermal regeneration and further elimination of the pollution that is transferred from liquid to solid phase (Gutkoski et al. 2024). Thus, the recycling of carbon-based materials used to trap pollutants from wastewater is a significant challenge because tons of polluted solid materials need to be treated. This is generally conducted at high temperatures (around 800 °C) and consumes an extensive amount of energy and time while also degrading the properties of the carbon adsorbents (Marques et al. 2017). Moreover, this thermal regeneration cannot be undertaken *in situ* since the process needs to be stopped so that the adsorption column can be transferred to a regeneration site, which increases the complexity and the global cost of the decontamination process.

Electrochemical regeneration of carbon-based adsorbents is gaining increasing attention as a promising alternative to conventional thermal methods, which are often energy-intensive and detrimental to the structural integrity of the materials (Ersan et al. 2023a; Ersan et al. 2024). Several recent studies have demonstrated the feasibility of restoring the adsorption capacity of carbon materials through *in situ* electrochemical processes, enabling oxidative degradation of retained pollutants directly on the adsorbent surface (Ersan et al. 2023a; Ersan et al. 2024). For instance, works by (Ding et al. (2020) and (Liu et al. (2020) highlighted the role of electrochemically generated oxidants, such as H_2O_2 or active oxygen species, in regenerating activated carbon. More recently, (Ersan et al. (2023b) and (Ferrández-Gómez et al. (2023) have shown that tailored electrochemical setups can significantly enhance regeneration efficiency, especially when combined with advanced oxidation processes. Despite these promising advances, electrochemical regeneration remains a relatively recent and evolving field, with ongoing investigations exploring the optimization of electrode materials (Gazigil et al. 2023; Hu et al. 2024), reactor configurations (Santos et al. 2022), and integration with photocatalytic or photoelectrochemical processes (Xing et al. 2016; Huang et al. 2017). These developments open new perspectives for sustainable and cost-effective reactivation of adsorbents in water treatment applications.

As explained above, many promising processes have been developed for the removal of ROCs but, individually, they present various drawbacks. The combination of several processes can reduce the drawbacks of a given technique owing to the advantages of each method (Cao et al. 2017). A combination of a carbon adsorbent, which increases the concentration of the micropollutant locally on the solid, followed by the use of OH radicals, could be used as a technique for *in situ* degradation of the adsorbed micropollutants while suppressing the need for high thermal treatments. To the best of our knowledge, this process of combining the adsorption of ROCs (by means of carbon xerogels) with *in situ* regeneration of the adsorbent using an electro-catalytic/UV technique is not currently reported in the literature.

The general goal of this work is to develop an innovative process for the removal of refractory organic compounds (ROCs) from water. The process is based on the adsorption of ROCs onto nanostructured carbons (carbon xerogels), coupled with *in situ* regeneration of the carbon adsorbent by H_2O_2 electro-generation, and an enhanced decomposition of ROCs by OH radicals due to UV illumination. The main goal of this work is to find a regeneration technique for the adsorbent material that replaces the thermal one typically used.

This process does not involve classical photocatalysis (no semiconductor excitation), but can be described as a **photo-assisted

electrochemical advanced oxidation process**, where **UV plays a catalytic role** in promoting radical formation. The combination of adsorption and electro/photo-oxidation enables pollutant removal and carbon regeneration in a single, reagent-free cycle.

The present paper mainly focuses on the carbon cathode development. First, carbon xerogels, *i.e.*, carbon materials with controlled *meso/* macropore size, are synthesized as centimeter-sized cylinders to be used as electrodes. Next, adsorption on these carbon xerogel cylinders is performed with three model pollutants (*i.e.*, methylene blue (MB), p-nitrophenol (PNP), and ibuprofen (IB)). Then, H_2O_2 electro-generation with these cylinders is studied as a possible regeneration method for the carbon xerogels. UV-A radiation is used during the H_2O_2 electro-generation to increase the decomposition of H_2O_2 into OH radicals and to accelerate the degradation of the adsorbed pollutants. Cylinders saturated with model pollutants are regenerated with this technique, showing the great potential of this novel process for carbon material regeneration and micropollutant removal.

2. Materials and methods

Materials: resorcinol (Merck, ACS reagent, ≥99.0 %, for synthesis), formaldehyde (37 % wt. in water, stabilized by 10–15 % wt. methanol, Sigma-Aldrich), distilled water, Na_2CO_3 (Acros Organics, 99.5 % extra pure, anhydrous), p-nitrophenol (ReagentPlus®, ≥99 %, Sigma-Aldrich), methylene blue (Reag. Ph Eur, Merck), ibuprofen (≥98 % (GC), powder, Sigma-Aldrich), sodium sulfate (ACS reagent, ≥99.0 %, anhydrous, granular, Sigma-Aldrich), Cerium (IV) sulfate ($Ce(SO_4)_2$, Sigma Aldrich), sulfuric acid (98 %, for analysis EMSURE®, Sigma-Aldrich), and hydrogen peroxide solution (30 % (w/w) in H_2O, contains stabilizer, Sigma-Aldrich).

2.1. Carbon xerogel preparation

Carbon xerogels were prepared according to a well-known polymerization-pyrolysis method described by Job et al. (Job et al. 2004), Wolfs et al. (Wolfs et al. 2022), and Karaman et al. (Karaman et al. 2024). Here, 1.725 mol of resorcinol (Merck, for synthesis) was dissolved in 20 mol of distilled H_2O under stirring (Wolfs et al. 2022). Next, a solution that contains 3.45 mol of formaldehyde (37 % wt. in water, stabilized by 10–15 % wt. methanol, Sigma-Aldrich), 8.24 mol of distilled H_2O, and 0.87 mol of methanol (from a formaldehyde solution 37 % wt. in water, stabilized by 10–15 % wt. methanol, Sigma-Aldrich) was added to the resorcinol solution (Wolfs et al. 2022). Finally, the pH was increased by adding a specific amount, C [mol], of Na_2CO_3 (Acros Organics, 99.5 % extra pure, anhydrous) (Wolfs et al. 2022). This quantity C is set by determining the molar ratio R/C, where R is the quantity of resorcinol (in mol) (Wolfs et al. 2022). The ratio R/C was set at four different values (*i.e.*, 100, 200, 750 and 1500) to control the pore texture of the materials. When Na_2CO_3 was dissolved in the precursor solution, 10 mL was poured into test tubes and sealed. Then, the tubes were placed inside an oven and heated to 85 °C for 72 h. Next, their caps were removed and the tubes were placed in a vacuum oven at 60 °C for 10 h; the temperature was then increased to 150 °C for 24 h. Finally, the gel was pyrolyzed under N_2 flux at 800 °C.

2.2. Adsorption experiments

To measure the adsorption of the three model pollutants (*i.e.*, MB, PNP, and IB) on the carbon cylinders, the pollutant was dissolved in a plastic container ($V_{H2O} = 500$ mL and $C_{MB} = 6$ mg/L, $C_{PNP} = 14$ mg/L, or $C_{IB} = 26$ mg/L). The adsorption tests only began after stirring the solution for 24 h to make sure that the adsorption of the pollutant by the container did not play a role. A blank test was also run, where the pollutant was placed in a container without any sample. The solutions were protected from ambient light throughout the test. Then, monoliths corresponding to different values of R/C were weighed and introduced to the container. Samples were taken regularly over several weeks to track the evolution of the pollutant concentration. The residual pollutant concentrations were determined using a spectrophotometry method (Genesys 150S UV–Vis spectrophotometer, Thermo Scientific), as described in Section 2.6.

2.3. H_2O_2 electro-generation experiments

The electro-generation of H_2O_2 with carbon cylinders was performed in a Plexiglas reactor with dimensions of 14.5 cm (length) × 6.4 cm (width) × 17.7 cm (height). The electrode combination (anode-cathode) employed was an IrO_2 grid-carbon cylinder. The distance between the electrodes was 1.5 cm. The anode and cathode were connected to the positive and negative outlets, respectively, of a digital DC generator, model 382,275 (EXTECH Instruments, Montréal, Canada). The current was set at 0.1, 0.3, or 0.5 A. The electrolyte medium was 500 mL of distilled water with 0.5 g/L of sodium sulfate. The experiment was performed for 1 h; the H_2O_2 concentration was measured every 10 min via cerium titration (Kiendrebeogo et al. 2022).

2.4. PNP plus H_2O_2 experiments with and without UV

To evaluate the impact of the UV light on the conversion of H_2O_2 to OH radicals, the degradation of p-nitrophenol (PNP) was studied with and without UV-A light (Osram Sylvania, Blacklight-Blue Lamp, F18W/BLB-T8, $\lambda = 365$ nm) in the presence of H_2O_2. Hence, two conditions were tested with three replications for each of them. Each sample consisted of a petri dish containing 25 mL of 14 mg/L PNP solution in water with 0.001 M of H_2O_2. The dishes were placed under the UV lamp or in the dark in a thermostatic box maintained at 20 °C; the solution was mixed via orbital stirring. The degradation of PNP was evaluated through absorbance measurements using a Genesys 150S UV–Vis spectrophotometer (Thermo Scientific) at $\lambda = 317$ nm, with spectra recorded over the range from 250 to 550 nm to examine the PNP degradation and to ensure the positions of the relevant peaks are included. The total organic carbon measurements (TOC-L CPN, Shimadzu, Kyoto, Japan) were also conducted to evaluate the mineralization of PNP.

2.5. Carbon cylinder regeneration experiments

For regeneration experiments, XC750 was selected as the optimal cathode material. For each pollutant, the same protocol was followed: three carbon cylinders were put into contact with a known amount of pollutant (14 mg for PNP, 6 mg for MB, and 26 mg for IB) in MilliQ water under stirring until complete adsorption of the pollutant was reached (*i.e.*, after 3 weeks). The complete adsorption was confirmed using UV–visible spectroscopy to obtain a spectrum with no adsorption peaks of the corresponding pollutants. Next, one cylinder was regenerated under the same conditions as detailed in Section 2.3, with a current of 0.1 A for several hours. During the regeneration process, the concentration of the electro-generated H_2O_2 was measured, the evolution of the pollutant and the by-product concentrations were analyzed via UV-visible spectroscopy and the amount of TOC in the water was measured at the end of the experiment. A second saturated cylinder was also regenerated under the same conditions but with UV illumination. A third saturated cylinder remained under stirring in the same water medium without applying a bias (*i.e.*, acting as a blank) to assess the eventual desorption of the pollutant. After the experiments, the three cylinders were exposed to the same amount of pollutants to evaluate their re-adsorption abilities.

To further understand the regeneration process, a non-porous carbon cylinder (XC100) that does not absorb pollutants was used in the electrochemical setup with the same amount of pollutants in the water. Their concentrations were determined via UV-visible spectroscopy. This experiment was undertaken with and without UV light.

2.6. Recycling experiments with the best form of carbon

Recycling experiments were undertaken with the best form of carbon. A known amount of PNP (500 mL at 14 mg/L) is put into contact with the optimal carbon cylinder and the remaining concentration after 24 h of contact is estimated (which is called the initial PNP adsorption capacity). Next, the carbon cylinder undergoes an electrochemical/UV regeneration with the optimal conditions (9 h at 0.1 A and under a UVA lamp of 18 W, an extra margin has been taken into account in the processing time to ensure complete pollutant degradation). After the treatment, the regenerated carbon is again put into contact with the PNP solution (500 mL at 14 mg/L) for 24 h to measure its adsorption capacity. It is undertaken five times in a row, with the PNP adsorption capacity measured after each regeneration. After five cycles of regeneration, the specific surface area is measured again.

This *in situ* regeneration method is compared with a thermal one. In the latter case, the optimal carbon cylinder is also put into contact with the PNP solution and then regenerated thermally in an alumina tubular oven (2 h at 800 °C under N_2). After the thermal regeneration, the thermally regenerated carbon is again put into contact with the PNP solution to measure the adsorption capacity. It is also undertaken five times and the specific surface area is measured after five cycles.

2.7. Analytical methods

The carbon cylinder samples were observed with a scanning electron microscope (SEM) using a TESCAN Clara microscope (high vacuum, 15 keV). The nitrogen adsorption-desorption isotherms were measured with an ASAP 2420 multi-sampler volumetric device (Micromeritics) at 196 °C; before the measurements, the samples were outgassed under a high vacuum (<2 μmHg) for 5 h at ambient temperatures, followed by 5 h at 105 °C (still under a high vacuum). From these isotherms, the specific surface area of the samples (S_{BET}) can be calculated. Mercury porosimetry measurements were undertaken with a Quantachrome Poremaster 60 from 0.01 to 400 MPa. From these measurements, the total intruded mercury volume, V_{Hg}, the macropore volume, V_{macro}, and the pore size distribution for pores larger than 3.8 nm from the Washburn equation (Pirard et al. 1998; Karaman et al. 2024) are obtained. The macropore volume is found by subtracting the compaction volume from the total intruded mercury volume.

A conductivity meter (Oakton Model 510) was used to determine the ionic conductivity of the effluent. Hydrogen peroxide (H_2O_2) concentrations were estimated using a cerium sulfate oxidation of the peroxide with ferrous orthophenatroline as the indicator (Kiendrebeogo et al. 2022). The residual concentrations of the pollutants (*i.e.*, MB, PNP, and IB) were determined via the absorbance measurements from a UV–Vis spectrophotometer (Genesys 150S UV–Vis spectrophotometer, Thermo Scientific). The maximum absorption of the samples of the MB solutions was measured at a wavelength of 665 nm, whereas the absorption peaks of the PNB and IB solution samples were determined at 317 nm and 225 nm, respectively. These adsorption peaks were identified to evaluate the progress of the pollutant removal from the solution. Calibration curves of known MB, PNB, and IB concentrations *versus* the absorption peaks (λ_{MB}, λ_{PNB}, and λ_{IB}, respectively) were used to evaluate the residual concentrations of the pollutants.

The total organic carbon (TOC) was measured using a Shimadzu TOC-L CPN analyzer (Shimadzu Scientific Instruments Inc.) equipped with an autosampler. The electrochemical impedance spectroscopy (EIS) analysis was performed at 0.1, 0.25, 0.5, and 1 mA on XC100 and XC750 samples. Data were collected in the frequency range of 100 mHz to 100 kHz with an amplitude of 10 % of the working current in a 0.5 g/L Na_2SO_4 solution. The EIS experiments were carried out using a three-electrode electrochemical cell (*i.e.*, a carbon cathode, a platinum grid, and a saturated calomel electrode (SCE) as a reference electrode) at ambient temperatures. An Autolab PGSTAT30 (Metrohm, Netherlands) potentiostat was used.

The toxicity tests were carried out according to the ISO 6341:2012 norm using *Daphnia magna*, a planktonic crustacean species bought from Microbiotests (Gent, Belgium, lot DM270224). The tests are described in the Supplementary Materials. These micro-crustaceans were exposed to seven different solutions: the three solutions of the pollutants before regeneration (with an initial concentration of 52 mg/L for IB, 12 mg/L for MB, and 28 mg/L for PNP), the three solutions of water after the regeneration using H_2O_2 and UV (one for each pollutant), and a solution corresponding to regeneration with only the H_2O_2 electro-generation (no UV irradiation) but solely for analyzing the condition of the PNP pollutant.

3. Results and discussion

3.1. Characterization of the xerogel carbon samples

Cylindrical carbon xerogels were synthesized from resorcinol and formaldehyde using a sol-gel process, varying the *R/C* ratio between 100 and 1500. Macroscopically, different aspects can be observed between the four cylinders: (i) XC100 is very dense, compact, and very difficult to break in two by hand, (ii) XC200 is still dense but seems more porous and can be broken by hand when applying high pressures, and (iii) XC750 and XC1500 have similar aspects, *i.e.*, very porous and solid, but are more easily breakable by hand.

Fig. 1 shows the adsorption-desorption isotherms for the four different cylinders. The textural information obtained from these measurements confirms what was observed visually. When the *R/C* ratio increased, the porosity of the samples was modified. At a low *R/C* ratio of 100, a non-porous material is obtained (Fig. 1 and Table 1) with a very low specific surface area (30 m^2/g). The porous structure tends to develop at higher *R/C* ratios. For example, the XC200 sample has a nitrogen adsorption-desorption isotherm of type I and IV (Lecloux 1971; Karaman et al. 2024) and the characteristics of microporous (a sharp adsorbed volume increase at low pressures) and mesoporous materials (hysteresis at higher pressures). The specific surface area at this ratio is estimated to be around 400 m^2/g (Table 1) whereas, at higher *R/C* ratios, the specific surface areas are around 600–700 m^2/g for XC750 and XC1500 (Table 1), indicating that they are mesoporous solids with type I isotherms (Lecloux 1971; Karaman et al. 2024). The microporous volume calculated from the nitrogen adsorption-desorption isotherms also follows the same tendency since S_{BET} mainly depends on microporosity.

Fig. 2 displays the mercury porosimetry curves for the four samples. Generally, two phenomena can be observed: (i) compaction of the material and (ii) intrusion of mercury into the pores. This change in behavior is characterized by an inflection point on increasing the

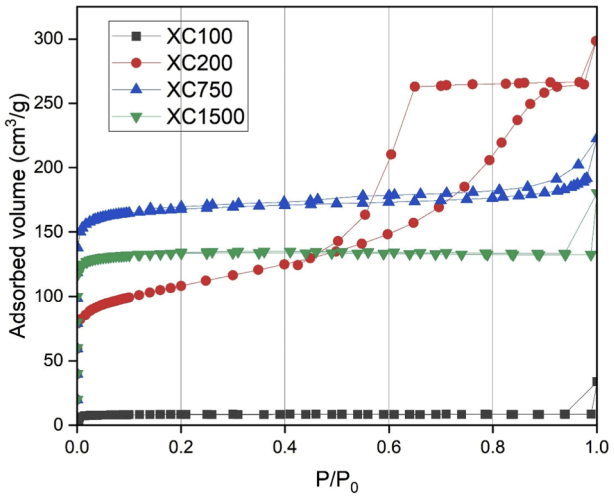

Fig. 1. Nitrogen adsorption-desorption isotherms for the four cylinders.

Table 1
Sample texture parameters.

Sample (*R/C*)	S_{BET} (m^2/g)	V_{micro} (cm^3/g)	V_p (cm^3/g)	V_{Hg} (cm^3/g)	V_{macro} (cm^3/g)	ε (-)
100	30	0.01	0.05	0.05	0	0.11
200	390	0.16	0.46	0.22	0.01	0.43
750	680	0.26	0.34	1.59	1.50	0.79
1500	550	0.21	0.28	1.85	1.80	0.80

Here, S_{BET} is the specific surface area calculated via the BET method, V_{micro} is the microporous volume calculated via the Dubinin-Radushkevich method (Job et al. 2004), V_P is the specific liquid volume adsorbed at the saturation pressure of nitrogen calculated from the nitrogen adsorption-desorption isotherm, V_{Hg} is the specific pore volume measured by mercury porosimetry, and ε is the porous fraction calculated from $\varepsilon = \frac{V_{Hg} + V_{micro}}{V_{Hg} + V_{micro} + \frac{1}{\rho_{carbon}}}$ (Deschamps et al. 2023), for which the density of carbon is set at 2 g/cm^3 (Deschamps et al. 2023).

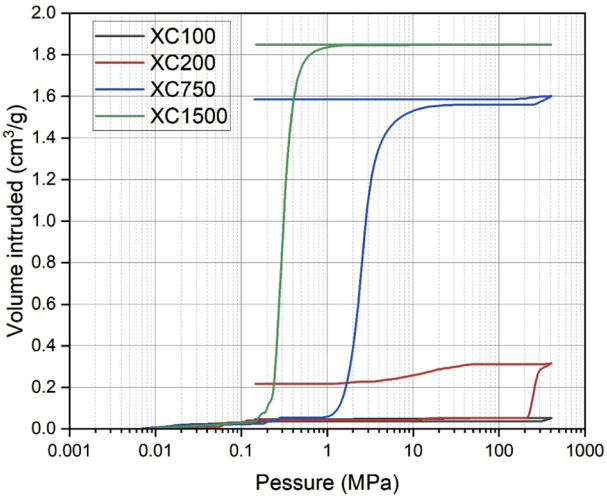

Fig. 2. Mercury porosimetry curves for the four cylinders.

pressure (Mahy et al. 2019a). XC100 effectively resists the mercury intrusion since only compaction is observed (black curve in Fig. 2), which results in a very dense, non-porous, and hard carbon material. The macroporous volume, V_{macro}, is null (Table 1). XC200 has a behavior similar to XC100 (*i.e.*, compaction) until a pressure of 200 MPa is reached, at which point a small intrusion of mercury is observed; thus, it is a resistant carbon material but with some porosity (a macroporous volume of around 0.01 cm^3/g; Table 1). As for the nitrogen adsorption-desorption isotherms, the XC750 and XC1500 samples have similar behaviors with compaction at low pressure (<1 MPa), then a high mercury intrusion leads to highly porous carbon with a macroporous volume of 1.50 cm^3/g and 1.80 cm^3/g, respectively (Table 1). The pore size distribution (Fig. 3) provides an average pore diameter of 6 nm, 570 nm, and 4700 nm for XC200, XC750, and XC1500, respectively. No pore distribution for XC100 is obtained (a non-porous material).

This modification of porosity is due to the different amounts of sodium carbonate that modify the pH of the medium and the formation of the carbon xerogel (Job et al. 2004; Job et al. 2005; Karaman et al. 2024). The higher the pH, the lower the *R/C* ratio and the smaller the carbon nodules formed, leading to dense and compact carbon materials. For a low pH (a high *R/C* ratio), large microporous carbon nodules are produced, resulting in porous carbon xerogels (Job et al. 2004; Job et al. 2005; Karaman et al. 2024). These explanations are confirmed by the SEM images of the carbon, which are displayed in Fig. 4. Similar morphology is obtained for all the samples with different spherical carbon nodule sizes, but only the sample with RC 100 is non-porous and

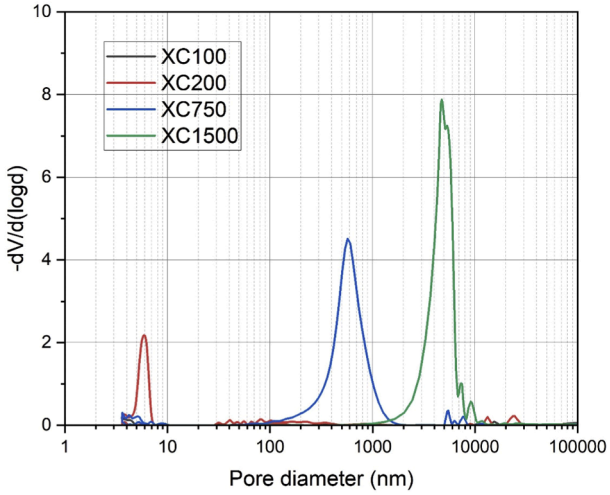

Fig. 3. Pore size distribution calculated from the mercury porosimetry data.

has a dense monolithic morphology (Figs. 4(a) and (b)). Typically, when the *R/C* ratio increases, the nodule size increases. Nevertheless, XC750 and XC1500 seem to have a similar nodule size (2–3 μm; Figs. 4(d) and 4 (e)).

3.2. Adsorption properties of XC cylinders

Section 3.1 showed that the four cylinders have different textures, from non-porous (XC100) to highly porous carbon material (XC750 and XC1500). The present section assesses the adsorption properties of these cylinders based on three different model pollutants: p-nitrophenol, methylene blue, and ibuprofen. These three pollutants are chosen because they represent three pollutant families that can be found at the exit of wastewater treatment plants as micropollutants, *i.e.*, pesticides, dyes, and pharmaceutical products. Moreover, these three types of pollutants were chosen to evaluate the versatility of the carbon cylinders to adsorb different kinds of pollutants, a property that a good adsorbent material must attain.

The PNP, MB, and IB adsorptions on the four cylinders are shown in Fig. 5. For PNP adsorption (Fig. 5(a)), the cylinders were able to absorb nearly all the pollutants after two days, except for XC100, which is non-porous (S_{BET} of 30 m^2/g, Table 1). For XC100, 10 % is adsorbed after seven days, but slow desorption is observed as the adsorption falls to 3 % after 28 days. XC200, which has mainly micropores and small mesopores (<10 nm), is still able to adsorb PNP quite quickly (>90 % after two days). PNP was rapidly removed (abatement >95 % after one day) using either XC750 or XC1500, which have the most porous cylinders. The rapid adsorption of PNP can be explained by its very small size (6.7 Å), allowing easy diffusion into small pores (<10 nm) and also a direct interaction with the surface group of the carbon cylinder.

In the case of the two other pollutants (Figs. 5(b) and (c)), complete adsorption is obtained after 30 days with the best-performing sample (XC750 in both cases). XC100 also has very weak adsorption for both molecules due to its low porosity, as discussed previously. The difference in adsorption between XC200 (with pores <10 nm) compared with XC750 and XC1500 (larger pore range; Fig. 3) is more important than in the case of PNP (Fig. 5(a)). The larger size of the MB and IB molecules (17 Å (Arias et al. 1999) and 13 Å (Mestre et al. 2007), respectively) can play a role in adsorption and diffusion in the pore network, which is larger in XC750 and XC1500, resulting in faster adsorption than XC200. For each cylinder, the time of adsorption is longer for MB and IB compared with PNP, probably because these two molecules are larger than PNP. These findings demonstrate the high versatility of carbon xerogels for adsorbing different molecules of various types.

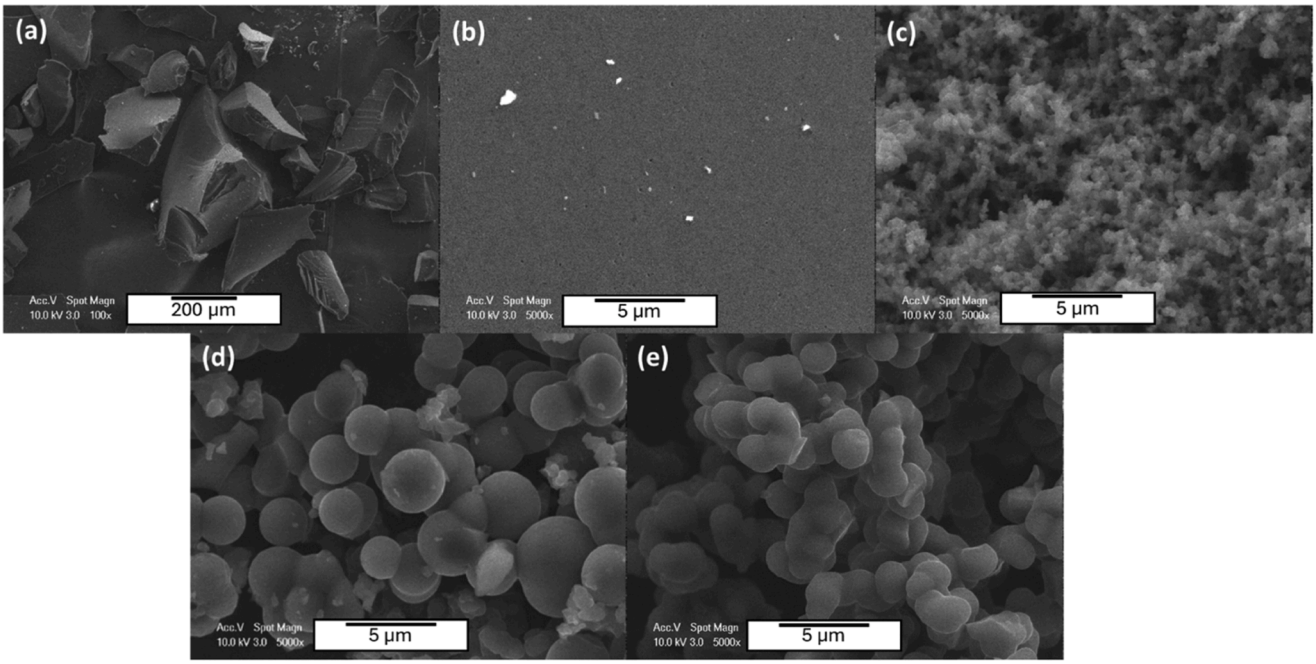

Fig. 4. SEM images of (a),(b) XC100, (c) XC200, (d) XC750, and (e) XC1500.

3.3. H_2O_2 electro-generation

The previous section has shown the possibility of the carbon cylinders adsorbing different kinds of pollutants. The goal of this paper is to set up an innovative method for saturated carbon regeneration to replace the usual thermal treatment. The innovation resides in the use of an electric current to generate oxidant molecules (H_2O_2) that can oxidize the molecules adsorbed on the carbon. This section determines the operation parameters for the electro-generation of H_2O_2 at the carbon cylinders.

The estimation of the H_2O_2 concentration in the liquid medium was performed using cerium titration (Kiendrebeogo et al. 2022). Previously, a calibration curve was made (Figure S1) to assess the H_2O_2 concentration between 0 and 20 mg/L. The calibration is considered reliable because the coefficient of determination (R^2) of the regression is 0.996.

For each cylinder, the H_2O_2 electro-generation capacity was estimated during 1 h of experimentation for four different currents. The evolution of the H_2O_2 concentration with time is represented in Fig. 6. For each cylinder, applying a current of 0.1 A provides the highest and the most stable H_2O_2 (red curves in Fig. 6). Moreover, the maximum concentration of H_2O_2 is different from one cylinder to another. The highest H_2O_2 concentrations (*i.e.*, 4.44 and 3.79 mg/L) after 1 h of electrolysis were recorded using XC750 and XC1500, respectively. Fig. 7 presents the maximal H_2O_2 concentration against the specific surface area, S_{BET}, of each cylinder. It is observed that the higher S_{BET}, the higher the maximal concentration of H_2O_2. When S_{BET} is higher, more adsorption and reaction sites are available for the oxygen reduction reaction, which can lead to greater H_2O_2 production (Yeager 1986; Trevelin et al. 2023). Since the XC750 cylinder showed the highest H_2O_2 electro-production and pollution adsorption, this sample was chosen for further investigation, *i.e.*, the *in situ* electro-regeneration experiments detailed in the next section.

This correlation between the surface area and H_2O_2 production can be attributed not only to an increased electroactive surface but also to the improved accessibility of oxygen at the catalytic sites, particularly in highly porous structures. Larger pore volumes and improved oxygen diffusion pathways facilitate the two-electron oxygen reduction reaction (ORR), leading to enhanced *in situ* H_2O_2 generation (Bokare and Choi 2014; Hu et al. 2024). Further studies could include the measurement of the Faradaic efficiency and the normalization of H_2O_2 production per electrode surface (or per *Ah*), as is undertaken in previous electro-regeneration works (Liu et al. 2020; Franz et al. 2020; Ding et al. 2020), for better comparisons with other systems.

The results for the electrochemical impedance spectroscopy (EIS) measurements are presented in two separate Nyquist plots (Figs. 8(a) and 8(b)), corresponding to two different carbon-based materials: a highly porous carbon (XC750) and a non-porous one (XC100), respectively.

At high frequencies, the intercept on the left-hand side of the Nyquist plot with the real axis (Z') typically reflects the electrolyte resistance (Bard and Faulkner 2001). In our case, a significantly higher interception is observed for the XC100 sample compared with XC750. Since the same electrolyte, setup, and reference/counter electrodes were used for both measurements, this discrepancy is unlikely to be due to differences in the electrolyte or cell configuration. Rather, it may stem from the lower volume of XC100. Although the mass of both samples was kept constant, the much higher porosity of XC750 results in a larger physical volume, which could reduce the local current density and apparent resistance.

At lower frequencies, the characteristic semicircle plots shown in Fig. 8(b), indicative of charge-transfer processes, are clearly observed for XC750, which points to a well-defined electrochemical interface (Bard and Faulkner 2001). For XC100, similar semicircles are also present but appear less defined and significantly larger, suggesting a much higher charge-transfer resistance. This observation is consistent with the lower surface area accessible for the electrolyte in XC100 due to its poor porosity. As a result, the electrochemical interface is less developed, which hinders charge transfer and explains the poorer electrochemical performance.

3.4. Effect of UV on the degradation potential of H_2O_2

In order to accelerate the carbon regeneration with electro-generated H_2O_2, a UV source was added to the process (Section 3.5). UV light converts H_2O_2 to OH radicals (Samuel et al. 2020), which have more capability to degrade organic molecules (Bokare and Choi 2014). To highlight the benefit of the use of UV, experiments were made by mixing one of the model pollutants (PNP) with H_2O_2 (10^{-3} M prepared solution)

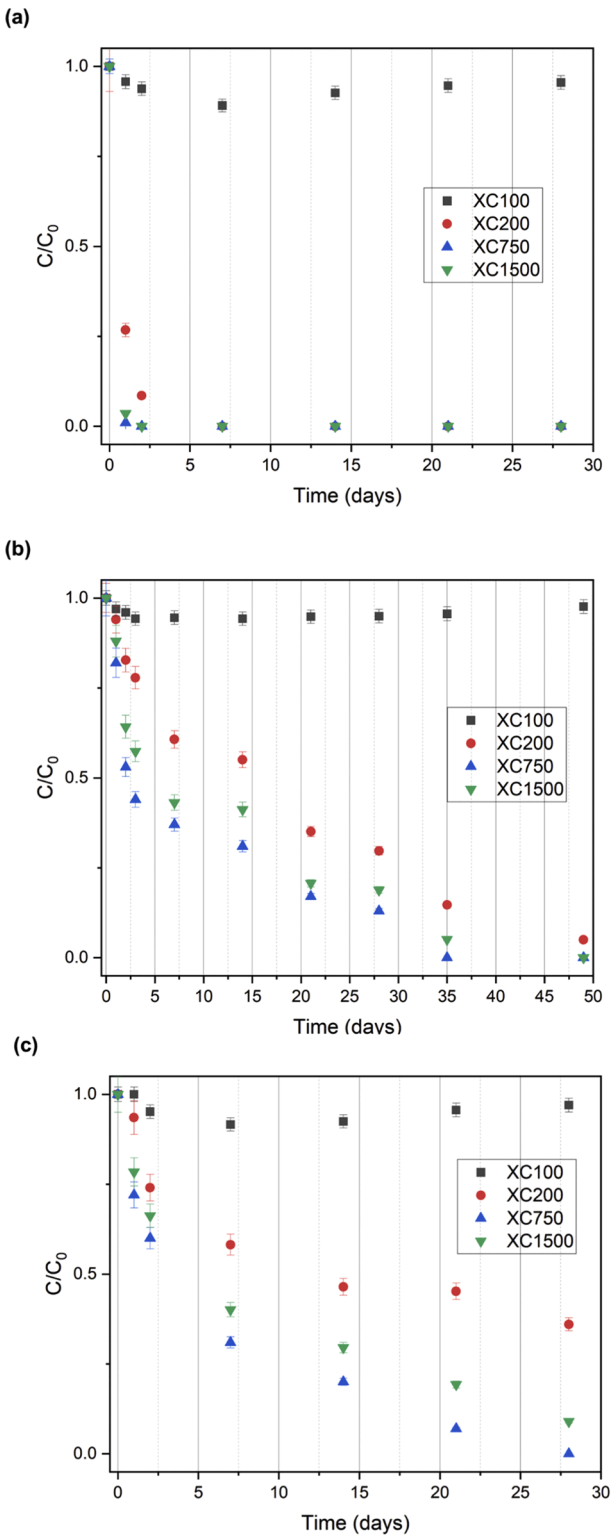

Fig. 5. Adsorption evolution over time for the four different carbon xerogel cylinders with (a) PNP, (b) MB, and (c) IB.

with and without UV light. The PNP concentration was measured after 2 h of reaction. The results are presented in Fig. 9. It is observed that after 2 h of reaction without UV, the PNP concentration has not changed while, with UV illumination, 15 % degradation is seen. This experiment confirms the utility of UV light in combination with H_2O_2 to degrade organic pollutants and that the OH radicals can efficiently mineralize these kinds of molecules (Eqs. (1) and (2)). Furthermore, PNP was also placed under UV light alone to ensure that no photolysis occurs, as shown in Fig. 9. The mechanism for the degradation of PNP by the hydroxyl radical was studied and fully described by (Paola et al. (2003); and Farcy et al. (2024): the C—NO_2 polarity bond, caused by the electron-withdrawing nature of the nitro group and the depletion of the carbon electron, enables the hydroxyl radical to attack this carbon, producing hydroquinone, which decomposes into benzoquinone, which the authors confirmed by GC–MS (Farcy et al. 2024). Next, the ring opening produces different species, leading to the mineralization of the unsought compound via the following reactions:

$$H_2O_2 + h\nu \rightarrow 2\ \bullet OH \quad (1)$$

$$PNP + \bullet OH \rightarrow \text{mineralization mechanism (Farcy et al. 2024)} \rightarrow CO_2 + H_2O \quad (2)$$

where h is the Planck constant (6.63×10^{-34} J s) and ν is the frequency of the input light (Hz).

The relatively limited degradation of PNP under UV-activated H_2O_2 (15 % in 2 h) without electrochemical generation highlights the importance of maintaining a constant oxidant supply. This suggests that the initial H_2O_2 concentration may have been insufficient to sustain radical-based degradation or that radical recombination (or scavenging) limited the reaction. These observations reinforce the benefit of continuous electrochemical generation of H_2O_2, which ensures a steady production of OH radicals for effective mineralization of the pollutants over time (Santos et al. 2022; Ersan et al. 2023a; Ersan et al. 2023b).

3.5. *In situ electro-regeneration of the optimal xerogel carbon samples*

In this section, the *in situ* process for carbon cylinder regeneration is assessed for the optimal carbon material, *i.e.*, XC750, with a known quantity of model pollutants adsorbed on its surface under three different conditions (as detailed in Section 2.6). In the first condition, the cylinder with a known amount adsorbed at its surface is placed into a freshwater medium and no desorption happens after 24 h of experimentation for the three pollutants, *i.e.*, nothing is detected in the medium after 24 h of contact. No peak associated with any species is detected with UV-visible spectroscopy for the three pollutants. For the two other conditions (H_2O_2 regeneration with and without UV light), the results with the three pollutants are presented in Fig. 10. For each pollutant, the evolution of the molecule amount in the solution is represented over time when the carbon cylinder is used as a cathode (continuous lines in Fig. 10). The concentration of H_2O_2 is also measured with cerium titration (square points in Fig. 10). The data in orange corresponds to the experiment with UV light and the data in blue without UV (Fig. 10). Moreover, in Table 2, the TOC measurement conditions at the end of the experiments are described alongside the corresponding TOC value if the total amount of the pollutant was in the solution. For the three pollutants, similar trends can be observed; the case of PNP will initially be discussed in more detail and then the parallels and differences between MB and IB will be examined.

For the PNP without UV (blue in Fig. 10(a)), the PNP amount in solution increases up to 240 min and then stays constant. The concentration of H_2O_2 increases during the experiment until 4 mg/L is reached, which is comparable to the value obtained when no pollutant is adsorbed (Fig. 6(c)). The amount of organic carbon at the end of the experiment is higher than the amount of PNP detected, suggesting that partial degradation occurs.

For the PNP with UV irradiation (orange in Fig. 10(a)), the PNP amount in solution increases up to 50 min, then decreases to zero. The concentration of H_2O_2 increases during the beginning part of the experiment, then falls and increases again when the amount of PNP decreases.

From these experiments, various observations and explanations can be drawn. (i) In both cases, the current passing through the system enables the desorption of PNP. (ii) When no UV light is applied, the

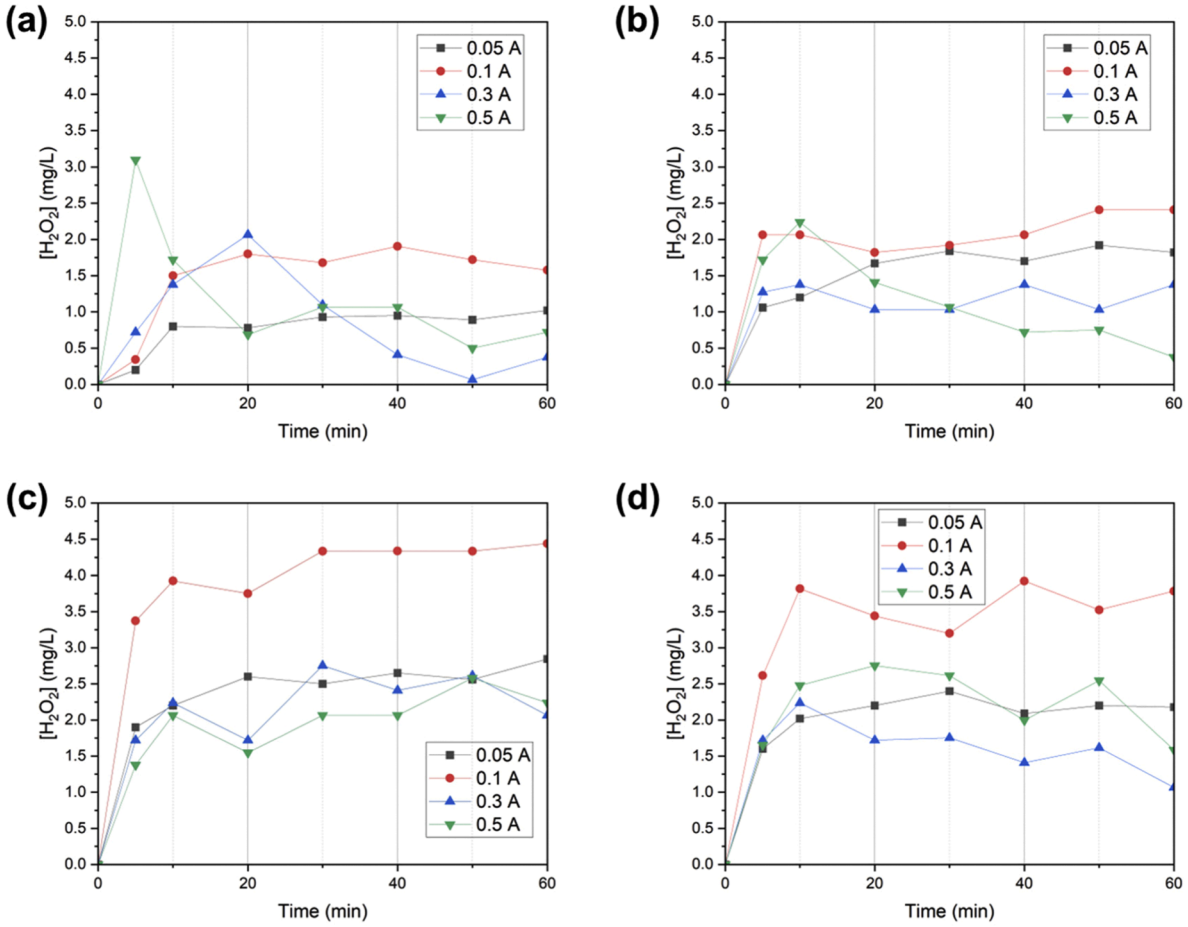

Fig. 6. H_2O_2 concentrations electro-generated in water solution between 0.05 and 0.5 mA with (a) XC100, (b) XC200, (c) XC750, and (d) XC1500 xerogel cylinders.

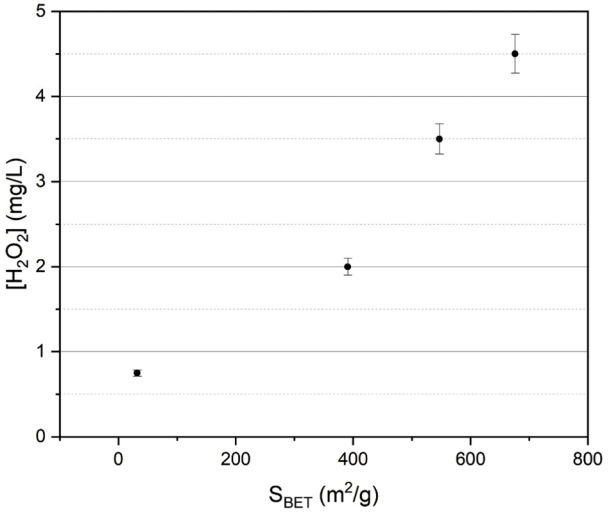

Fig. 7. Maximal concentration of H_2O_2 electro-produced as a function of the specific surface area, S_{BET}.

desorption is slower and stabilizes at a certain value. The concentration of H_2O_2 at the end of the experiment suggests that all the PNP is desorbed since the concentration is close to the level measured without pollutants (Fig. 6(c)). PNP was partially degraded by the electro-oxidation process. In fact, the TOC at the end of the experiment is lower than the initial value, which suggests degradation, but the detection of PNP at the end of the experiment is lower than the initial concentration—the TOC is, thus, composed of PNP and degradation products. (iii) When UV light is used, complete degradation of the PNP is obtained. The TOC value can be considered to be zero, so total mineralization of the pollutants occurs. Moreover, no PNP is detected.

The difference between the experiment with and without UV light can be explained as follows. (i) When there is no illumination, H_2O_2 is produced at the cathode alongside different gases due to water electrolysis (Trevelin et al. 2023). This phenomenon enables the desorption of the pollutant. Due to the dual-electrode system, the pollutant can undergo oxidation reactions and be partially degraded (Rekik et al. 2024). The H_2O_2 produced can also play a role in this degradation, but H_2O_2 alone is not sufficiently powerful to fully degrade it (Mahy et al. 2023). At the endpoint, the pollutant is desorbed from the carbon support and the pollutant is partially degraded, but by-products are present in the solution. (ii) With UV light, the pollutant is also desorbed due to the water electrolysis reactions but, in this case, the electro-produced H_2O_2 can be converted to OH radicals that are able to fully mineralize the pollutant (Mahy et al. 2023). At this endpoint, the carbon surface is regenerated and the pollutants are mineralized (Table 2).

Similar mechanisms can be observed with MB (Fig. 10(b)) and IB (Fig. 10(c)). For MB, an enhancement of MB degradation is also observed when UV light is used. Nevertheless, even without light, the molecule is fully degraded. The production of OH radicals accelerates the degradation (Mahy et al. 2023). For IB, the behavior is very similar to that of PNP. Without light, the IB is partially degraded due to the electro-oxidation process, but only a small part is mineralized (Table 2). With UV light, total degradation is observed. The time taken for total degradation is longer for IB compared with PNP because the IB molecule

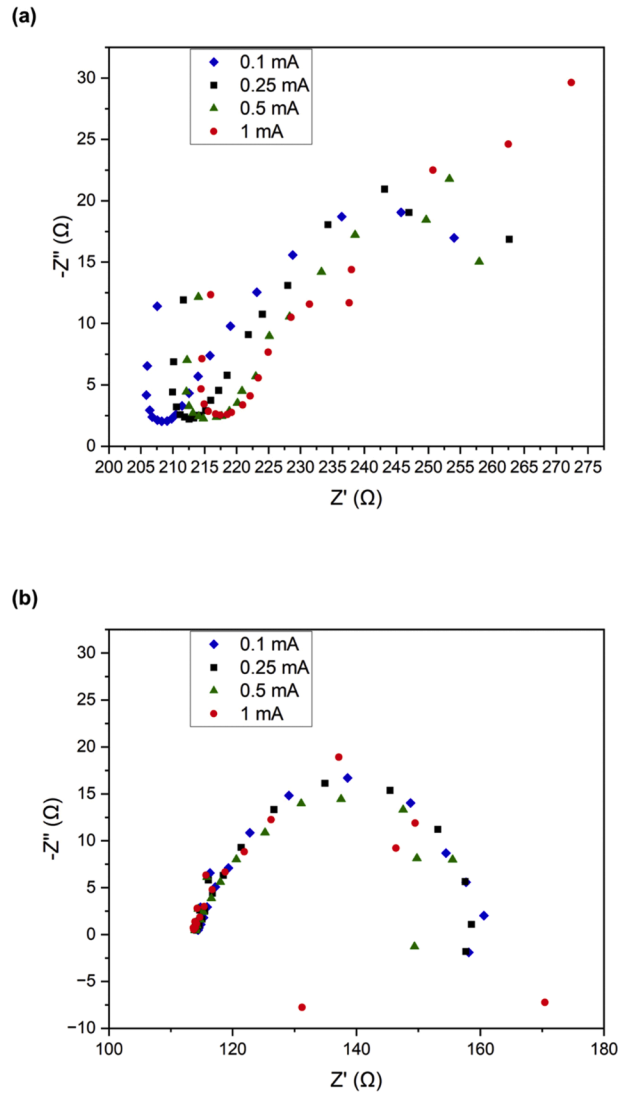

Fig. 8. Nyquist plot obtained for (a) XC100 and (b) XC750 at 0.1, 0.25, 0.5, and 1 mA.

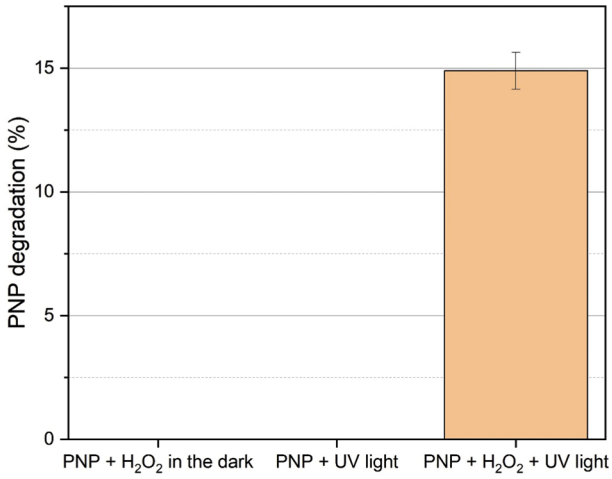

Fig. 9. PNP degradation (%) after 2 h of reaction with or without H_2O_2 and with and without UV light.

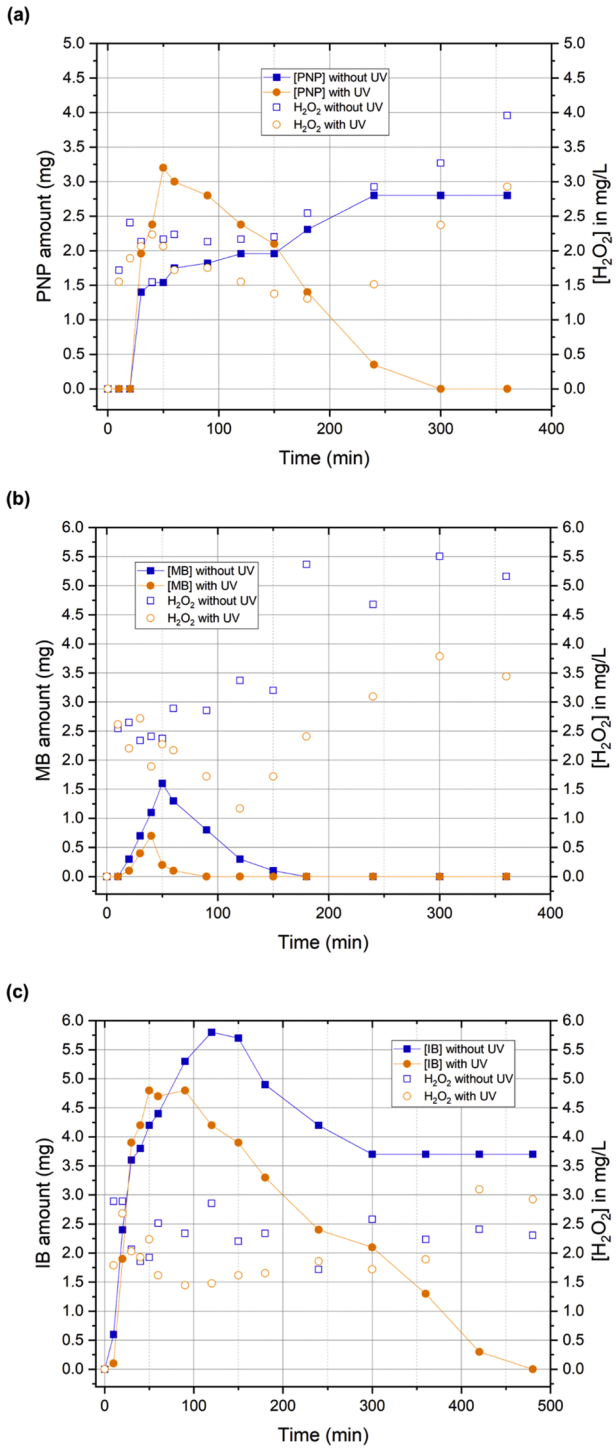

Fig. 10. Evolution of (a) PNP, (b) MB, or (c) IB amounts over time during the H_2O_2 regeneration experiments with or without UV illumination, with XC750 as the carbon cathode. The continuous line corresponds to the concentration of the pollutant and the square dots indicate the concentration of H_2O_2. The blue-filled squares are the data without UV, and the orange-filled circles are the data with UV. The experiments were undertaken in triplicate, but the error bars (comprised of 2.2 and 3.4 %) were not added in order to avoid overloading the figures with data.

is more complex to degrade (Balseviciute et al. 2025). In order to confirm the efficiency of the process of combining H_2O_2 electro-generation with UV light, and that the degradation of the three pollutants is not due to the re-adsorption of the initial molecules and

Table 2
TOC values at the end of the *in situ* regeneration experiments and for the initial conditions.

Conditions	TOC (mg/L)
14 mg of PNP in 0.5 L (volume of reaction medium)	16.7
PNP, current, and no light	13.3
PNP, current, and UV light	<0.5
6 mg of MB in 0.5 L (volume of reaction medium)	6.4
MB, current, and no light	<0.5
MB, current, and UV light	<0.5
26 mg of IB in 0.5 L (volume of reaction medium)	27.1
IB, current, and no light	23.5
IB, current, and UV light	<0.5

by-products on the porous carbon cathode, similar experiments were conducted where a non-porous carbon cathode (XC100) was used instead of XC750, with the pollutants entered directly into the solutions. In this case, no adsorption can occur because the carbon cathode is not porous. The results for the three pollutants are presented in Fig. 11.

The results depicted in Fig. 11 confirm the results shown in Fig. 10, *i.e.*, the H_2O_2 electro-generation without UV light allows partial degradation and the degradation rate increases when UV light is added. The rate of degradation is slower in Fig. 11 compared with Fig. 10 for all the pollutants, which likely relates to the concentration of the electro-produced H_2O_2 that is lower for XC100 compared with XC750 (Fig. 6, which shows more than double the concentration for XC750 *versus* XC100). Particularly for the experiment under UV light, where the amount of H_2O_2 is linked to the amount of OH radicals that can be produced, in the case of XC100, fewer OH radicals can be produced compared with XC750, leading to a slower degradation rate.

Although the formation of hydroxyl radicals (•OH) is not directly evidenced by EPR spectroscopy in this study, their generation is strongly supported by the degradation efficiency observed and by the well-established role of UV-activated H_2O_2 in promoting •OH formation in similar systems (Hu et al. 2024). Future work will include EPR analysis to provide direct identification of the reactive species involved and further elucidate the degradation mechanism.

To evaluate the integrity of the carbon cathode after the electro-regeneration process, the XC750 sample was examined with SEM microscopy (Fig. 12). A comparison with a fresh XC750 sample (Fig. 4(d)) shows that the morphology of the sample remains identical, and no apparent degradation can be observed.

Finally, the ecotoxicity of the water medium before and after regeneration treatment (both H_2O_2 electro-generation and UV light) was assessed using *Daphnia magna* microcrustaceans (Section 2.7). The results of the experiments are presented in Table 3.

The three pollutants have different toxicities. With the initial concentrations (Table 3, before treatment), the order of toxicity is as follows: IB < PNP < MB. In contrast, the order of the mass concentration is the opposite, with MB having the lowest concentration (12 mg/L).

For the three pollutants, the toxicity of the solution decreases after the regeneration treatment (H_2O_2 and UV), showing the benefit of this treatment. For PNP, the water resulting from the regeneration treatment with only the electro-generation of H_2O_2 (Table 3) shows that intermediate by-products are still present. Thus, it is clear that the inclusion of UV irradiation is necessary to obtain the required degradation of the PNP molecules. This confirms the obtained results (Figs. 10(a) and 11(a)), indicating that intermediate molecules are produced that are not degraded by the H_2O_2 alone.

While the combination of electro-generated H_2O_2 and UV light led to significant toxicity reduction, residual effects could still be observed for high pollutant concentrations. This could be attributed to the presence of intermediate oxidation by-products, which are not always fully mineralized. The identification and monitoring of such by-products using advanced analytical techniques (*e.g.*, LC-MS or GC–MS) would help better understand their contribution to toxicity and further refine the treatment process (Ding et al. 2020).

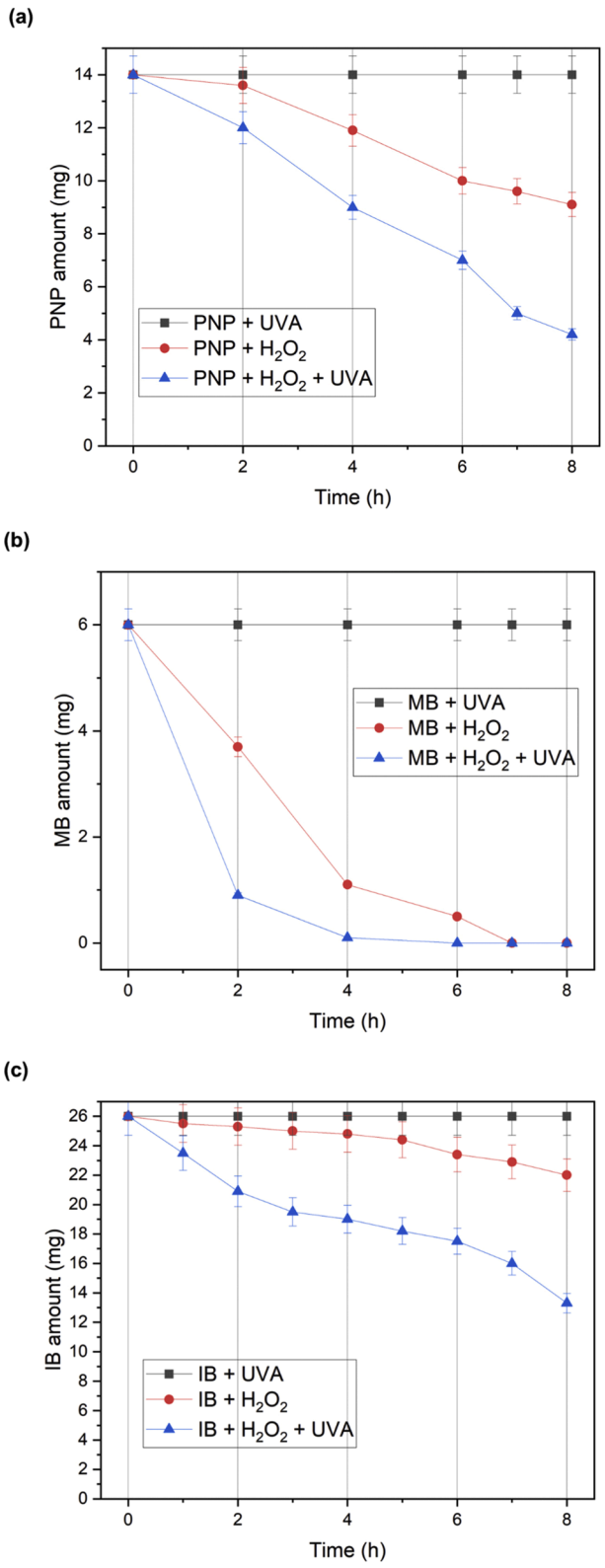

Fig. 11. Evolution of (a) PNP, (b) MB, or (c) IB amounts over time during the H_2O_2 electro-generation experiments with and without UV illumination, with XC100 as the carbon cathode.

In order to provide additional insight into the degradation phenomena involved during the electrochemical/UV regeneration process, a general description of the expected reaction pathways mediated by

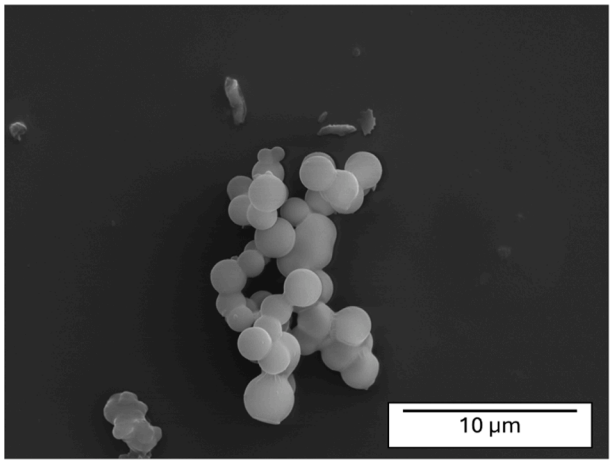

Fig. 12. SEM image of XC750 after the UV electro-regeneration process.

hydroxyl radicals is presented below.

Although a full mechanistic study was beyond the scope of this work, the degradation of organic micropollutants by hydroxyl radicals (•OH) is well-documented in the literature (Pignatello et al. 2006; Bokare and Choi 2014). Generally, •OH radicals are highly reactive, non-selective oxidants that initiate pollutant breakdown via several pathways: electrophilic addition to aromatic rings, hydrogen abstraction from aliphatic chains, and subsequent oxidative fragmentation of the molecular structure (Pignatello et al. 2006; Bokare and Choi 2014). For aromatic compounds such as p-nitrophenol and methylene blue, •OH attack typically leads to ring-opening reactions and progressive oxidation into smaller intermediates, ultimately resulting in complete mineralization to CO_2 and H_2O (Pignatello et al. 2006; Bokare and Choi 2014). Similarly, ibuprofen undergoes •OH-mediated degradation through hydroxylation, decarboxylation, and cleavage of the aromatic moiety (Pignatello et al. 2006; Bokare and Choi 2014). The complete removal of TOC and the reduction of ecotoxicity observed in this study are consistent with such radical-driven mineralization pathways.

3.6. Regeneration cycles

The long-term efficiency and durability of the carbon xerogel regeneration process were assessed over five consecutive adsorption-regeneration cycles using the XC750 sample. Two regeneration strategies were compared: (i) the *in situ* electrochemical/UV regeneration developed in this study and (ii) a conventional thermal regeneration carried out at 800 °C for 2 h under a N_2 atmosphere. After each cycle, the adsorption performance was evaluated based on the amount of p-nitrophenol (PNP) adsorbed in fresh solution after 24 h of contact.

As shown in Fig. 13, the adsorption capacity of the UV-electro-regenerated carbon remained remarkably stable over the five cycles, indicating that the material maintained its adsorption performance. In contrast, the thermally regenerated sample showed a progressive decrease in adsorption efficiency, dropping by >20 % after five cycles. This loss in performance is consistent with the degradation of the porous structure observed via N_2 adsorption-desorption isotherms (Fig. 14). Indeed, the specific surface area (S_{BET}) of the fresh carbon was 680 m^2/g, slightly decreasing to 645 m^2/g after five electrochemical/UV regeneration cycles (a 5 % loss), while the thermally regenerated sample exhibited a drastic reduction to 430 m^2/g (a 37 % loss). The two samples were also weighed before and after the five cycles; the UV-electro-regenerated carbon kept exactly the same mass, while the thermal regenerated one lost 30.5 % of its mass.

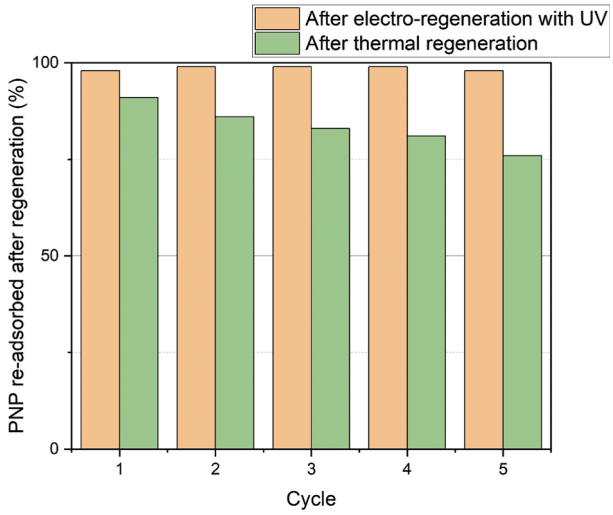

Fig. 13. PNP adsorption percentage after 24 h of contact between each regeneration cycle: UV electro-regeneration process (orange bar) and thermal regeneration process (green bar).

Table 3
Percentage immobilization of *Daphnia magna* for the three pollutants under different conditions.

PNP	Time (h)	C0 (reference) 0	C5 12.5 %	C4 25 %	C3 50 %	C2 75 %	C1 100 %
Before treatment	24	10	25	70	100	100	100
(% immobilization)	48	10	65	100	100	100	100
After H_2O_2 only	24	0	100	100	100	100	100
(% immobilization)	48	–	–	–	–	–	–
After H_2O_2 and UV	24	5	0	5	5	10	20
(% immobilization)	48	5	10	10	20	25	40
MB	Time (h)	C0 (reference) 0	C5 12.5 %	C4 25 %	C3 50 %	C2 75 %	C1 100 %
Before treatment	24	5	100	100	100	100	100
(% immobilization)	48	-	-	-	-	-	-
After H_2O_2 and UV	24	0	0	0	5	10	40
(% immobilization)	48	0	0	5	25	65	95
IB	Time (h)	C0 (reference) 0	C5 12.5 %	C4 25 %	C3 50 %	C2 75 %	C1 100 %
Before treatment	24	5	0	0	0	15	35
(% immobilization)	48	5	0	5	5	35	50
After H_2O_2 and UV	24	0	0	5	5	5	10
(% immobilization)	48	5	0	5	5	5	10

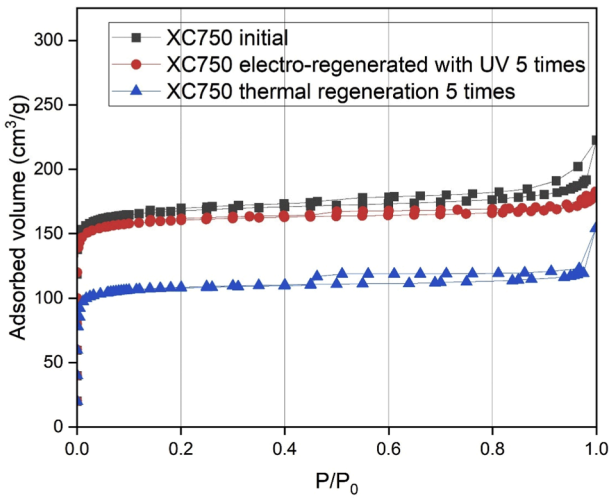

Fig. 14. Nitrogen adsorption-desorption isotherms for the XC750 samples: after synthesis (■), after five cycles of the UV electro-regeneration process (●), and after five cycles of the thermal regeneration process (▲).

This contrast highlights a major advantage of the developed electrochemical process: regeneration occurs at room temperature, avoiding the thermal stress that damages pore structure and surface chemistry. Moreover, the electro-regeneration strategy is *in situ* and reagent-free, thus eliminating the need for off-site treatment and reducing both operational complexity and environmental footprint. The UV-activated H_2O_2 generated electrochemically enables the complete mineralization of adsorbed pollutants, as confirmed by the TOC and ecotoxicity measurements, and avoids accumulation of the transformation by-products or residual toxicity.

An estimation of the energy consumption under laboratory conditions revealed a clear advantage for the electrochemical/UV regeneration process, with a total energy use of 0.1683 kWh per cycle, compared with 2.793 kWh for thermal regeneration (see Supplementary Materials for the calculational details). This represents a reduction of approximately 94 % in energy consumption. Such a difference is particularly significant when considering the scaling-up for continuous operation or repeated regeneration cycles. In addition to preserving the structural integrity of the adsorbent, the lower energy footprint of the electro-regeneration process offers a major advantage in terms of environmental impact and operational cost, aligning with current objectives in sustainable water treatment technologies. Comparable electrochemical AOP systems reported in the literature typically consume between 1 and 3 kWh/m^3 for water treatment (Liu et al. 2020; Ding et al. 2020), which positions our system as an energetically favorable solution, particularly given its reagent-free nature.

Altogether, these results confirm that the UV-assisted electrochemical regeneration process not only matches but outperforms thermal regeneration in terms of preserving adsorbent performance and material integrity over multiple cycles. These advantages position the approach as a promising, sustainable, and scalable alternative for real-world applications in water treatment systems relying on the adsorptive removal of micropollutants.

These results not only confirm the viability of the electro-regeneration process as an efficient alternative to thermal treatment but also demonstrate its potential for more sustainable applications. The absence of high-temperature requirements avoids structural degradation of the adsorbent, while the *in situ* generation of reactive species eliminates the need for chemical additives, thus simplifying operational logistics and reducing environmental impact (Gazigil et al. 2023; Ferrández-Gómez et al. 2023).

To synthesize on the overall process developed in this study: This process can be divided into two sequential and complementary stages. First, organic micropollutants are captured by adsorption onto the porous carbon xerogel monoliths. This step relies on the high surface area and hydrophobicity of the material, allowing the pollutants to be efficiently retained at the surface and within the pore network.

Once saturated, the carbon monolith is subjected to an *in situ* regeneration step, during which a cathodic current is applied in an oxygenated electrolyte. This triggers the electrochemical reduction of dissolved oxygen into hydrogen peroxide (H_2O_2) at the surface of the carbon material, which serves as both adsorbent and cathode. Simultaneously, UV illumination is applied to activate the generated H_2O_2 into hydroxyl radicals (•OH), which are highly reactive oxidants capable of degrading and mineralizing the adsorbed pollutants.

This process does not involve classical photocatalysis (no semiconductor excitation), but can be described as a photo-assisted electrochemical advanced oxidation process, where UV plays a catalytic role in promoting radical formation. The combination of adsorption and electro/photo-oxidation enables pollutant removal and carbon regeneration in a single, reagent-free cycle.

3.7. Comparison with the literature

A comparative overview of recent regeneration strategies for carbon-based adsorbents is presented in Table 4. While such comparisons are insightful, it is important to emphasize that strict benchmarking remains difficult due to the significant variability in experimental parameters—such as the nature and concentration of pollutants, adsorbent properties, electrode materials, applied currents, regeneration durations, and electrolyte compositions. Despite these differences, several trends can be highlighted that underline the originality and efficiency of the present work.

For instance, (Ding et al. (2020) regenerated phenol-loaded carbon fibers using an electro-peroxymonosulfate (PMS) process (1 A, [PMS] = 75 mM, 6 h), achieving 82.5 % regeneration after one cycle but with notable degradation over time—only 60 % capacity after ten cycles and a drop in S_{BET} to 280 m^2/g. (Liu et al. (2020) used an electro-peroxydisulfate system on activated carbon fibers (1 A, [PDS] = 100 mM), with a regeneration efficiency of just 34 % after four cycles and a surface area reduction to 390 m^2/g. In contrast, (Hu et al. (2024) obtained promising results using activated persulfate at 50 °C, achieving 80 % regeneration after five cycles, though at the cost of elevated temperature and chemical consumption. (Huang et al. (2017) also combined persulfate with electrochemical and Fe(II) activation but reached only 40 % regeneration after three cycles, under relatively high voltage and reagent doses.

Other studies have explored electro-regeneration under milder conditions. (Santos et al. (2022) maintained the adsorption capacity of methylene blue on activated carbon over eight cycles at 0.1 A, but with an initial surface area of only 385 m^2/g. (Gazigil et al. (2023) reported a progressive decline in efficiency from 100 % to 68 % over six cycles despite using advanced electrode materials (*i.e.*, Sn/Sb/Ni–Ti and Pt/Ti). (Ferrández-Gómez et al. (2023) successfully regenerated granular activated carbon from real water treatment applications using 0.025 A/cm^2 for 4 h in a H_2SO_4 electrolyte, recovering 90 % of the original surface area after a single cycle. More complex methods, such as that used by (Chistyakov et al. (2021)—combining microwave treatment, chemical soaking, and thermal activation—preserved adsorption capacity after one cycle but led to a decrease in the surface area from 616 to 500 m^2/g.

Compared with these studies, the present work offers several advantages. Our *in situ* electro-regeneration strategy—coupled with UV irradiation—achieves complete mineralization of three model pollutants (*i.e.*, p-nitrophenol, methylene blue, and ibuprofen) within 9 h at a low current (0.1 A), under ambient temperatures and without external oxidants or chemical additives. The structural integrity of the carbon xerogel is preserved over at least five cycles, with the surface area decreasing only slightly from 680 to 645 m^2/g. Additionally, the dual

Table 4
Comparison with the literature.

Reference	Type of adsorbent	Pollutant	Conditions of optimal regeneration	Results
This study	Carbon xerogel (680 m^2/g)	p-nitrophenol Methylene blue Ibuprofen	*In situ* electro-regeneration coupled with UV for 9 h under 0.1 A.	After five cycles, the adsorption property is maintained (S_{BET} = 645 m^2/g) *versus* thermal regeneration decreased by 24 % (S_{BET} = 430 m^2/g)
(Chistyakov et al. 2021)	Porous carbon modified with iron (616 m^2/g)	m-cresol	Microwave treatment under CO_2 followed by ammonium hydroxide aqueous solution soaking and drying, then 400 °C for 30 min	After one cycle, the adsorption properties stay the same, but S_{BET} decreases to 500 m^2/g
(Ding et al. 2020)	Carbon fiber (875 m^2/g)	Phenol	Electro-peroxymonosulfate (PMS) process with a current of 1A for 6 h, the concentration of PMS is 75 mM	Regeneration of 82.5 % after the first cycle and still 60 % after ten cycles (S_{BET} = 280 m^2/g)
(Ersan et al. 2023b)	Granular activated carbon, F400 (1039 m^2/g)	Perfluorooctanoic acid	*In situ* electro-regeneration at 1 mA with Ti anode from 1 h to 168 h of regeneration	Regeneration maintained over four cycles
(Gazigil et al. 2023)	Activated carbon (coal-based carbon)	Methylene blue	Electro-regeneration with Sn/Sb/Ni-Ti cube as anode and Pt/Ti as cathode, at 50 mA/cm^2 for 4 h	Adsorption efficiency moves from 100 % to 68 % after six cycles
(Hu et al. 2024)	Porous carbon (1300 m^2/g)	Tylosin	Activated persulfate regeneration with 3 mM at 50 °C	After five cycles, still 80 % of the carbon is regenerated
(Huang et al. 2017)	Granular activated carbon, F400 (1100 m^2/g)	Phenol	Persulfate/electrochemical/$FeCl_2$ process with 2 g/L and 1 g/L of persulfate and $FeCl_2$, respectively, and 22.5 V between Ti anode and stainless-steel cathode during 12h	40 % of the regeneration after three cycles
(Liu et al. 2020)	Activated carbon fiber (952 m^2/g)	Phenol	electro-peroxydisulfate process with 1 A, the concentration of PDS is 100 mM, and the Ti/Pt electrode is used for 6 h	34 % of the regeneration after four cycles (S_{BET} = 390 m^2/g)
(Santos et al. 2022)	Activated carbon (385 m^2/g)	Methylene blue	Electro-regeneration with CFC cathode and Ti/$Ru_{0.3}Ti_{0.7}O_2$ anode, 0.1 A for 2 h	Adsorption capacity maintained for eight cycles (300 m^2/g)
(Xing et al. 2016)	Carbon (XC-72 from Cabot, 186 m^2/g)	Acid Orange 7 (AO7), Ponceau 2R, and Rhodamine B	Solvent regeneration with ethanol/water mixture for 3 h	Regeneration comprised between 63 % and 78 % depending on the dye for one cycle of regeneration
(Ferrández-Gómez et al. 2023)	Granular activated carbon (Filtrasorb®TL820 and Norit1020®, 950 m^2/g)	Used three years in a drinking water treatment plant (organic pollutants of various types)	Electro-regeneration with 0.025 A/cm^2 for 4 h with H_2SO_4 electrolyte.	Regeneration of 90 % after one cycle (based on the resulting S_{BET} with a value of 885 m^2/g)

functionality of the monolithic xerogel—as both adsorbent and cathode—simplifies the system and enhances the sustainability of the process. These features highlight the relevance and innovation of our approach and position it as a viable and environmentally friendly alternative to thermal or chemically intensive regeneration techniques.

3.8. Challenges and recommendations

While the results obtained in this study demonstrate the effectiveness of the electrochemical/UV regeneration strategy for carbon xerogels, several challenges remain before practical implementation at a larger scale can be envisioned. One of the primary limitations lies in the scalability of the current setup, which is based on monolithic carbon electrodes operated under low current densities and controlled laboratory conditions. Although promising results were obtained with a relatively simple two-electrode configuration, the translation to pilot or full-scale systems would require the design of reactors compatible with flow-through operation, optimized current distribution, and effective light penetration throughout the electrode material. Previous studies, such as Liu et al. (2020) and Ding et al. (2020), have already highlighted the importance of cell geometry, hydrodynamics, and mass transport limitations when moving from batch to continuous systems for the electro-regeneration processes.

Another key aspect is the cost-efficiency of the process. Unlike thermal regeneration, which involves high energy consumption and significant structural degradation of the adsorbent, the electrochemical approach operates at ambient temperature, thus reducing energy demand. Moreover, the use of oxygen-saturated water and *in situ* generation of H_2O_2 avoids the need for chemical oxidants. However, UV irradiation and electricity consumption still represent operational costs that must be optimized through improved electrode design and possible solar-assisted alternatives, as proposed by (Ersan et al. (2023b). Additionally, the durability of the adsorbent over extended cycles must be further validated, particularly in real wastewater matrices where the presence of competing substances or fouling agents can affect both adsorption and electrochemical reactivity (Ferrández-Gómez et al. 2023). Future studies should also investigate the influence of water matrix parameters such as pH, ionic strength, and the presence of competing ions, in order to assess the robustness and applicability of the regeneration process in real water treatment scenarios.

This study addresses several of these challenges by demonstrating the following:(i) the dual functionality of carbon xerogels as an adsorbent and a cathode, simplifying system architecture; (ii) a high regeneration efficiency without external reagents; (iii) material stability over multiple cycles, as supported by surface area retention and TOC removal data.

Nevertheless, further research is required to develop modular reactor designs with scalable configurations (*e.g.*, stacked or flow-through cells), investigate the influence of real water matrices (including the presence of ions, and biofilms), evaluate techno-economic feasibility under different energy scenarios and pollutant loads, and explore alternative light sources or coupling with photovoltaic systems for sustainable UV activation (Hu et al. 2024).

In conclusion, while this work provides a strong proof-of-concept for sustainable and efficient *in situ* regeneration of carbon adsorbents, continued efforts in process integration, cost analysis, and field validation are crucial for moving toward practical implementation in industrial wastewater treatment systems.

4. Conclusion

Carbon xerogel cylinders were successfully synthesized via a sol-gel route, with their specific surface area tunable through the resorcinol/carbonate (*R/C*) ratio. Higher *R/C* ratios led to more porous structures and improved adsorption performance, as confirmed with three model pollutants: p-nitrophenol, methylene blue, and ibuprofen. These monolithic xerogels also served as efficient cathodes for *in situ* H_2O_2 electro-generation, reaching up to a H_2O_2 concentration of 5 mg/L for

the most porous sample (XC750), with performance improving at lower currents and higher surface areas. UV illumination further enabled the conversion of H_2O_2 into •OH radicals, enhancing the degradation efficiency of the adsorbed pollutants.

The combined electrochemical/UV regeneration strategy proved effective for fully mineralizing the three pollutants adsorbed onto the carbon. While methylene blue can be fully degraded without UV, PNP and IB require UV activation to achieve mineralization and reduced energy consumption. Ecotoxicity tests using *Daphnia magna* confirmed a significant reduction in toxicity after treatment. A comparison with thermal regeneration highlighted the beneficial effect of electro-regeneration on maintaining the adsorption properties.

This work demonstrates, for the first time, the potential of carbon xerogels as dual-function materials for pollutant adsorption and *in situ* electrochemical regeneration, offering a promising, reagent-free alternative to thermal regeneration for micropollutant removal in water treatment.

Funding

Julien G. Mahy thanks the F.R.S.-FNRS for his Postdoctoral Researcher position. J.G.M. is also grateful to the Rotary for a District 2160 grant, to the University of Liège and the FNRS for financial support for a postdoctoral stay of one year at INRS Centre Eau, Terre, Environnement in Québec, Canada.

CRediT authorship contribution statement

Julien G. Mahy: Writing – review & editing, Writing – original draft, Validation, Methodology, Investigation, Funding acquisition, Formal analysis, Conceptualization. **Hamed Arab:** Writing – review & editing, Supervision, Methodology, Investigation, Formal analysis. **Marthe Kiendrebeogo:** Writing – review & editing, Investigation, Formal analysis. **Antoine Farcy:** Writing – review & editing, Investigation, Formal analysis. **Tom Servais:** Formal analysis, Investigation, Writing – review & editing. **Alexandre Léonard:** Writing – review & editing, Investigation, Formal analysis. **Patrick Drogui:** Writing – review & editing, Supervision, Project administration, Methodology, Funding acquisition, Formal analysis.

Declaration of competing interest

The authors declare that they have no known competing financial interests or personal relationships that could have appeared to influence the work reported in this paper.

Acknowledgments

Julien G. Mahy thanks the F.R.S.-FNRS for his Postdoctoral Researcher position. J.G.M. is also grateful to the Rotary for a District 2160 grant, to the University of Liège, and to the FNRS for financial support for a postdoctoral stay at INRS Centre Eau, Terre, Environnement in Québec, Canada. The authors acknowledge Pr. Stéphanie Lambert and Pr. Nathalie Job for their fruitful discussions. The authors thank the CARPORVISU platform of the University of Liège and its manager, Dr. Alexandre Léonard, for the mercury porosimetry measurements.

Data availability statement

The raw/processed data required to reproduce these findings can be shared on demand.

Ethical approval

The authors declare that they have no known competing financial interests or personal relationships that could have appeared to influence the work reported in this paper.

Consent to participate

All authors agreed to participate in this work.

Consent to publish

All authors agreed to this version for publication.

Supplementary materials

Supplementary material associated with this article can be found, in the online version, at doi:10.1016/j.hazadv.2025.100742.

Data availability

Data will be made available on request.

References

Adeleye, A.S., Xue, J., Zhao, Y., Taylor, A.A., Zenobio, J.E., Sun, Y., Han, Z., Salawu, O. A., Zhu, Y., 2022. Abundance, fate, and effects of pharmaceuticals and personal care products in aquatic environments. J. Hazard. Mater. 424. https://doi.org/10.1016/j.jhazmat.2021.127284.

Ammar, A., 2023. «À peine de quoi boire » : Dans la bande de Gaza, les enfants sont privés de 90 % de leurs besoins en eau. Unicef.

Arias, M., López, E., Nunez, A., Rubinos, D., Soto, B., Barral, M.T., Diaz-Fierros, F., 1999. Adsorption of methylene blue by red mud, an oxide-rich byproduct of bauxite refining. In: Berthelin (Ed.), Effect of Mineral-Organic-Microorganisms on Soil and Freshwater Environments. Kluwer Academic/Plenum, New York, pp. 361–365.

Balseviciute, A., Patiño-Cantero, I., Carrillo-Abad, J., Giner-Sanz, J.J., García-Gabaldón, M., Pérez-Herranz, V., MC, Martí-Calatayud, 2025. Degradation of multicomponent pharmaceutical mixtures by electrochemical oxidation: insights about the process evolution at varying applied currents and concentrations of organics and supporting electrolyte. Sep. Purif. Technol. 362. https://doi.org/10.1016/j.seppur.2025.131697.

Bard, A.J., Faulkner, L.R., 2001. Electrochemical methods : fundamentals and applications, 2nd edition. John Wiley & Sons, Inc.

Bashir, N., Sawaira, T., Jamil, A., Awais, M., Habib, A., Afzal, A., 2024. Challenges and prospects of main-group metal-doped TiO2 photocatalysts for sustainable water remediation. Mater. (Basel) Today Sustainability 27. https://doi.org/10.1016/j.mtsust.2024.100869.

Bokare, A.D., Choi, W., 2014. Review of iron-free Fenton-like systems for activating H2O2 in advanced oxidation processes. J. Hazard. Mater. 275, 121–135. https://doi.org/10.1016/j.jhazmat.2014.04.054.

Brovini, E.M., Moreira, F.D., Martucci, M.E.P., de Aquino, S.F., 2023. Water treatment technologies for removing priority pesticides. J. Water (Basel) Process Eng. 53. https://doi.org/10.1016/j.jwpe.2023.103730.

Cao, D., Wang, Y., Zhao, X., 2017. Combination of photocatalytic and electrochemical degradation of organic pollutants from water. Curr. Opin. Green. Sustain. Chem. 6, 78–84. https://doi.org/10.1016/j.cogsc.2017.05.007.

Chistyakov, A.V., Liberman, E.Y., Pasevin, V.I., Bondarenko, G.N., Arapova, O.V., Tsodikov, M.V., 2021. Regeneration of a porous iron-containing carbon adsorbent under plasma-catalytic conditions assisted by microwave irradiation. Petroleum Chem. (Easton) 61 (4), 498–503. https://doi.org/10.1134/S0965544121050078.

Corson-Dosch, H., Nell, C., Volentine, R.E., Archer, A.A., Bechtel, E., Bruce, J.L., Felts, N., Gross, T.A., Lopez-Trujillo, D., Riggs, C.E., Read, E.K., Survey, U.S.G., 2023. The water cycle. Reston, VA.

Deschamps, F.L., Mahy, J.G., Léonard, A.F., Job, N., 2023. Rotating disk electrode measurements on low and high loading catalyst layers: diffusion limitations and application to Pt catalysts supported on porous micrometric carbon xerogel particles designed for proton exchange membrane fuel cells. J. Electroanalytical Chem. (Easton) 933, 117279. https://doi.org/10.1016/j.jelechem.2023.117279.

Din, M.I., Khalid, R., 2025. Photocatalysis of pharmaceuticals and organic dyes in the presence of silver-doped TiO2 photocatalyst–A critical review. Int. J. Environ. Anal. Chem. 105 (2), 276–300. https://doi.org/10.1080/03067319.2023.2258795.

Ding, H., Zhu, Y., Wu, Y., Zhang, J., Deng, H., Zheng, H., Liu, Z., Zhao, C., 2020. In situ regeneration of phenol-saturated activated carbon Fiber by an electro-peroxymonosulfate process. Environ. Sci. Technol. 54 (17), 10944–10953. https://doi.org/10.1021/acs.est.0c03766.

Ersan, G., Cerrón-Calle, G.A., Ersan, M.S., Garcia-Segura, S., 2023a. Opportunities for in situ electro-regeneration of organic contaminant-laden carbonaceous adsorbents. Water (Basel) Res 232. https://doi.org/10.1016/j.watres.2023.119718.

Ersan, G., Ersan, M.S., Perreault, F., Garcia-Segura, S., 2023b. Enabling in situ electro-regeneration systems for PFOA-laden spent activated carbon adsorbents reuse. J. Environ. Chem. Eng. 11 (6). https://doi.org/10.1016/j.jece.2023.111369.

Ersan, G., Gaber, M.S., Perreault, F., Garcia-Segura, S., 2024. Comparative study on electro-regeneration of antibiotic-laden activated carbons in reverse osmosis concentrate. Water (Basel) Res. 255. https://doi.org/10.1016/j.watres.2024.121528.

Farcy, A., Mahy, J.G., Alié, C., Caucheteux, J., Poelman, D., Yang, Z., Eloy, P., Body, N., Hermans, S., Heinrichs, B., Lambert, S.D., 2024. Kinetic study of p-nitrophenol degradation with zinc oxide nanoparticles prepared by sol–gel methods. J. Photochem. Photobiol. a Chem. 456. https://doi.org/10.1016/j.jphotochem.2024.115804.

Ferrández-Gómez, B., Martínez-Sánchez, B., Cazorla-Amorós, D., Morallón, E., 2023. Effect of concentration and flow rate of electrolyte on electrochemical regeneration of activated carbon at pilot-plant scale. J. Electroanalytical Chem. (Easton) 946. https://doi.org/10.1016/j.jelechem.2023.117727.

Franz, S., Arab, H., Chiarello, G.L., Bestetti, M., Selli, E., 2020. Single-step preparation of large area TiO2 photoelectrodes for water splitting. Adv. Energy Mater. 10 (23). https://doi.org/10.1002/aenm.202000652.

Gazigil, L., Er, E., Yonar, T., 2023. Determination of the optimum conditions for electrochemical regeneration of exhausted activated carbon. Diam. Relat. Mater. 133. https://doi.org/10.1016/j.diamond.2023.109741.

Guitaya, L., Drogui, P., Blais, J.F., 2015. In situ reactive oxygen species production for tertiary wastewater treatment. Environ. Sci. Pollution Res. 22 (9), 7025–7036. https://doi.org/10.1007/s11356-014-3907-3.

Gutkoski, J.P., Schneider, E.E., Michels, C., 2024. How effective is biological activated carbon in removing micropollutants? A comprehensive review. J. Environ. Manage 349, 119434.

Hu, Z., Cai, J., Song, G., Tian, Y., Zhou, M., 2021. Anodic oxidation of organic pollutants: anode fabrication, process hybrid and environmental applications. Curr. Opin. Electrochem. 26. https://doi.org/10.1016/j.coelec.2020.100659.

Hu, Z., Wang, J., Tie, M., Zhu, J., Sharaf, F., 2024. Enhanced adsorption of tylosin by ordered multistage porous carbon and efficient in-situ regeneration of saturated adsorbents by activated persulfate oxidation: performance, mechanism and multiple cycles. Environ. Pollution 361. https://doi.org/10.1016/j.envpol.2024.124861.

Huang, X., An, D., Song, J., Gao, W., Shen, Y., 2017. Persulfate/electrochemical/FeCl2 system for the degradation of phenol adsorbed on granular activated carbon and adsorbent regeneration. J. Clean. Prod. 165, 637–644. https://doi.org/10.1016/j.jclepro.2017.07.171.

Ip, A.W.M., Barford, J.P., McKay, G., 2010. A comparative study on the kinetics and mechanisms of removal of Reactive Black 5 by adsorption onto activated carbons and bone char. Chem. Eng. J. 157 (2–3), 434–442. https://doi.org/10.1016/j.cej.2009.12.003.

Issaka, E., AMU-Darko, J.N.O., Yakubu, S., Fapohunda, F.O., Ali, N., Bilal, M., 2022. Advanced catalytic ozonation for degradation of pharmaceutical pollutants–a review. Chemosphere 289. https://doi.org/10.1016/j.chemosphere.2021.133208.

Job, N., Pirard, R., Marien, J., Pirard, J.P., 2004. Porous carbon xerogels with texture tailored by pH control during sol-gel process. Carbon. N. Y. 42 (3), 619–628. https://doi.org/10.1016/j.carbon.2003.12.072.

Job, N., Théry, A., Pirard, R., Marien, J., Kocon, L., Rouzaud, J.N., Béguin, F., Pirard, J. P., 2005. Carbon aerogels, cryogels and xerogels: influence of the drying method on the textural properties of porous carbon materials. Carbon. N. Y. 43 (12), 2481–2494. https://doi.org/10.1016/j.carbon.2005.04.031.

Karaca, S., Gürses, A., Açikyildiz, M., Ejder (Korucu), M., 2008. Adsorption of cationic dye from aqueous solutions by activated carbon. Microporous Mesoporous Mater (Basel) 115 (3), 376–382. https://doi.org/10.1016/j.micromeso.2008.02.008.

Karaman, B., Tonnoir, H., Huo, D., Carré, B., Léonard, A.F., Gutiérrez, J.C., Piedboeuf, M. L., Celzard, A., Fierro, V., Davoisne, C., Janot, R., Job, N., 2024. CVD-coated carbon xerogels for negative electrodes of Na-ion batteries. Carbon. N. Y. 225. https://doi.org/10.1016/j.carbon.2024.119077.

Kiendrebeogo, M., Karimi Estahbanati, M.R., Ouarda, Y., Drogui, P., Tyagi, R.D., 2022. Electrochemical degradation of nanoplastics in water: analysis of the role of reactive oxygen species. Sci. Total. Environ. 808, 151897. https://doi.org/10.1016/j.scitotenv.2021.151897.

Lecloux, A., 1971. Exploitation des isothermes d'adsorption et de désorption d'azote pour l'étude de la texture des solides poreux. Mémoires Société Royale des Sciences de Liège, pp. 169–209.

Liu, Z., Ren, B., Ding, H., He, H., Deng, H., Zhao, C., Wang, P., Dionysiou, D.D., 2020. Simultaneous regeneration of cathodic activated carbon fiber and mineralization of desorbed contaminations by electro-peroxydisulfate process: advantages and limitations. Water (Basel) Res 171. https://doi.org/10.1016/j.watres.2019.115456.

Mahy, J.G., Kiendrebeogo, M., Farcy, A., Drogui, P., 2023. Enhanced decomposition of H2O2 using metallic silver nanoparticles under UV/visible light for the removal of p-nitrophenol from water. Catalysts. 13 (5), 842. https://doi.org/10.3390/catal13050842.

Mahy, J.G., Lambert, S.D., Léonard, G.L.M., Zubiaur, A., Olu, P.Y., Mahmoud, A., Boschini, F., Heinrichs, B., 2016. Towards a large scale aqueous sol-gel synthesis of doped TiO2: study of various metallic dopings for the photocatalytic degradation of p-nitrophenol. J. Photochem. Photobiol. a Chem. 329, 189–202. https://doi.org/10.1016/j.jphotochem.2016.06.029.

Mahy, J.G., Tasseroul, L., Tromme, O., Lavigne, B., Lambert, S.D., 2019a. Hydrodechlorination and complete degradation of chlorinated compounds with the coupled action of Pd/SiO<inf>2</inf>and Fe/SiO<inf>2</inf>catalysts: towards industrial catalyst synthesis conditions. J. Environ. Chem. Eng. 7 (2), 103014. https://doi.org/10.1016/j.jece.2019.103014.

Mahy, J.G., Wolfs, C., Mertes, A., Vreuls, C., Drot, S., Smeets, S., Dircks, S., Boergers, A., Tuerk, J., Lambert, S.D., 2019b. Advanced photocatalytic oxidation processes for micropollutant elimination from municipal and industrial water. J. Environ. Manage 250. https://doi.org/10.1016/j.jenvman.2019.109561.

Marques, S.C.R., Marcuzzo, J.M., Baldan, M.R., Mestre, A.S., Carvalho, A.P., 2017. Pharmaceuticals removal by activated carbons: role of morphology on cyclic thermal regeneration. Chem. Eng. J. 321, 233–244. https://doi.org/10.1016/j.cej.2017.03.101.

Mestre, A.S., Pires, J., Nogueira, J.M.F., Carvalho, A.P., 2007. Activated carbons for the adsorption of ibuprofen. Carbon. N. Y. 45 (10), 1979–1988. https://doi.org/10.1016/j.carbon.2007.06.005.

Oturan, M.A., Aaron, J.J., 2014. Advanced oxidation processes in water/wastewater treatment: principles and applications. A review. Crit. Rev. Environ. Sci. Technol. 44 (23), 2577–2641. https://doi.org/10.1080/10643389.2013.829765.

Páez, C.A., Contreras, M.S., Léonard, A., Blacher, S., Olivera-Fuentes, C.G., Pirard, J.P., Job, N., 2012. Effect of CO 2 activation of carbon xerogels on the adsorption of methylene blue. Adsorption 18 (3–4), 199–211. https://doi.org/10.1007/s10450-012-9394-2.

Paola A Di, Augugliaro V., Palmisano L., Pantaleo G., Savinov E. (2003) Heterogeneous photocatalytic degradation of nitrophenols. 155:207–214.

Pignatello, J.J., Oliveros, E., MacKay, A., 2006. Advanced oxidation processes for organic contaminant destruction based on the fenton reaction and related chemistry. Crit. Rev. Environ. Sci. Technol. 36 (1), 1–84. https://doi.org/10.1080/10643380500326564.

Pirard, R., Heinrichs, B., Van Cantfort, O., Pirard, J.P., 1998. Mercury porosimetry applied to low density xerogels; relation between structure and mechanical properties. J. Solgel. Sci. Technol. 13 (1), 335–339. https://doi.org/10.1023/A:1008676211157.

Rekik, H., Pichon, L., Teymoorian, T., Arab, H., Sauvé, S., El Khakani, M.A., Drogui, P., 2024. Efficient electro-oxidation-based degradation of per- and polyfluoroalkyl (PFAS) persistent pollutants by using plasma torch synthesized pure-Magnéli phase-Ti4O7 anodes. J. Environ. Manage 370. https://doi.org/10.1016/j.jenvman.2024.122929.

Samuel, M.S., Jose, S., Selvarajan, E., Mathimani, T., Pugazhendhi, A., 2020. Biosynthesized silver nanoparticles using Bacillus amyloliquefaciens; application for cytotoxicity effect on A549 cell line and photocatalytic degradation of p-nitrophenol. J. Photochem. Photobiol. B 202. https://doi.org/10.1016/j.jphotobiol.2019.111642.

Sanavi Fard, M., Ehsani, A., Soleimani, F., 2023a. Treatment of synthetic textile wastewater containing Acid Red 182 by electro-peroxone process using RSM. J. Environ. Manage 344. https://doi.org/10.1016/j.jenvman.2023.118379.

Sanavi Fard, M., Ehsani, A., Soleimani, F., 2023b. Optimization of toluenediamine degradation in synthetic wastewater by a UV/H2O2 process using full factorial design. Water (Basel) Resour. Ind. 30. https://doi.org/10.1016/j.wri.2023.100218.

Santos, D.H.S., Santos, J.P.T.S., Duarte, J.L.S., Oliveira, L.M.T.M., Tonholo, J., Meili, L., Zanta, C.L.P.S., 2022. Regeneration of activated carbon adsorbent by anodic and cathodic electrochemical process. Process Saf Environ. Protect. 159, 1150–1163. https://doi.org/10.1016/j.psep.2022.01.083.

Scholz, N., 2016. Setting criteria on endocrine disruptors: follow-up to the General Court judgment. Brief Eur. Parliament 1–10. April.

Trench, A.B., Moura, J.P.C., VS, Antonin, Gentil, T.C., Lanza, M.R.V., Santos, M.C., 2023. Using a novel gas diffusion electrode based on Vulcan XC-72 carbon modified with Nb2O5 nanorods for enhancing H2O2 electrogeneration. J Electroanalytical Chem. (Easton) 946. https://doi.org/10.1016/j.jelechem.2023.117732.

Trevelin, L.C., Valim, R.B., Lourenço, J.C., De Siervo, A., Rocha, R.S., Lanza, M.R.V., 2023. Using ZrNb and ZrMo oxide nanoparticles as catalytic activity boosters supported on Printex L6 carbon for H2O2 production. Adv. Powder Technol. (Singap. World Sci.) 34 (9). https://doi.org/10.1016/j.apt.2023.104108.

Turolla, A., Fumagalli, M., Bestetti, M., Antonelli, M., 2012. Electrophotocatalytic decolorization of an azo dye on TiO 2 self-organized nanotubes in a laboratory scale reactor. Desalination. 285, 377–382. https://doi.org/10.1016/j.desal.2011.10.029.

Undeman, E., Rasmusson, K., Kokorite, I., Leppänen, M.T., Larsen, M.M., Pazdro, K., Siedlewicz, G., 2022. Micropollutants in urban wastewater: large-scale emission estimates and analysis of measured concentrations in the Baltic Sea catchment. Mar. Pollut. Bull. 178. https://doi.org/10.1016/j.marpolbul.2022.113559.

UNESCO, 2022. PHI-IX : plan stratégique du Programme hydrologique intergouvernemental de l'UNESCO: la science pour un monde où la sécurité de l'eau est assurée dans un environnement en mutation. Neuvième Phase 2022–2029.

United Nations Educational S and CO, 2021. Rapport mondial des Nations Unies sur la mise en valeur des ressources en eau 2021. United Nations.

Wolfs, C., Lambert, S.D., Léonard, A.F., Mahy, J.G., 2022. Custom-shaped carbon Xerogel materials by 3D printing. Processes 10 (10), 1979. https://doi.org/10.3390/pr10101979.

Xing, X., Qu, H., Chen, P., Chi, B., Xie, H., 2016. Studies on competitive adsorption of dyes onto carbon (XC-72) and regeneration of adsorbent. Water (Basel) Sci. Technol. (Singap. World Sci.) 74 (10), 2505–2514. https://doi.org/10.2166/wst.2016.413.

Yeager, E., 1986. Dioxygen electrocatalysis: mechanisms in relation to catalyst structure. J. Mol. Catal. 38, 5–25.

Yu, J.X., Li, B.H., Sun, X.M., Yuan, J., an, ChiR, 2009. Polymer modified biomass of baker's yeast for enhancement adsorption of methylene blue, rhodamine B and basic magenta. J. Hazard. Mater. 168 (2–3), 1147–1154. https://doi.org/10.1016/j.jhazmat.2009.02.144.

Zhang, M., Yan, J., Wang, D., Dong, X., Ma, H., Wei, H., Wang, G., 2023a. Anodic water oxidation to H2O2 on Fe-doped ZnO for electro-Fenton wastewater purification. Electrochim. Acta 464, 142940. https://doi.org/10.1016/j.electacta.2023.142940.

Zhang, M., Yan, J., Wang, D., Dong, X., Ma, H., Wei, H., Wang, G., 2023b. Anodic water oxidation to H2O2 on Fe-doped ZnO for electro-Fenton wastewater purification. Electrochim. Acta 464. https://doi.org/10.1016/j.electacta.2023.142940.